processes

MDPI

*Article*

# A Study on the Film Superposition Method for the Multi-Row Film Cooling of the Turbine Outer Ring

**Ziqiang Gao [1], Tian Qiu [1,*], Peng Liu [1,*], Shuiting Ding [1], Zongchao Li [2], Ronghui Cheng [2] and Qiyu Yuan [1]**

[1] Research Institute Pof Aero-Engine, Shahe Campus, Beihang University, 9 Nansan Street, Shahe Higher Education Park, Changping District, Beijing 102206, China; ziqiang@buaa.edu.cn (Z.G.); dst@buaa.edu.cn (S.D.); zb2132111@buaa.edu.cn (Q.Y.)
[2] AECC Shenyang Engine Research Institute, Shenyang 110015, China; lizongchao1989@163.com (Z.L.); rhcheng_gte@sina.com (R.C.)
* Correspondence: qiutian@buaa.edu.cn (T.Q.); liupeng91@buaa.edu.cn (P.L.)

**Abstract:** The film superposition prediction model is a crucial tool in the preliminary design of the turbine outer ring, enabling the rapid estimation of adiabatic wall temperatures and significantly reducing computational costs. This study established the relationship between the mainstream temperature correction coefficient and the air bleed ratio based on energy conservation principles in the boundary layer during film injection. A superposition model grounded in mainstream temperature corrections was developed. The proposed model utilizes cooling efficiency characteristics based on the equivalent blowing ratio to accurately predict the cooling efficiency of multi-row hole layouts with varying hole spacings. Experiments on the adiabatic film cooling efficiency were conducted with four different hole configurations at various blowing ratios. The limitations of the traditional Sellers superposition method in predicting cooling efficiency distributions are discussed by comparing them with experimental data. The comparison reveals that the Sellers method accumulates prediction errors as the number of hole rows increases, leading to an overestimation of the cooling efficiency. Introducing a mainstream temperature correction factor effectively addressed this issue. The prediction accuracy of the improved model was higher at $M = 0.3$, with relative deviations remaining within 10% across different test plates. As the blowing ratio increased, the prediction deviation gradually increased when the number of hole rows was less than 10. At a blowing ratio of 1.0, the deviation exceeded 20%. However, as the number of hole rows increased, the deviation remained within 10% under various blowing ratios. Compared to existing advanced models in the literature, the improved model demonstrated higher prediction accuracy under most conditions. For Case 1 in this study, the model predicted an average surface cooling efficiency deviation of 3.4% at a blowing ratio of 0.5. Similarly, for Case 14 in the literature, the deviation was 3.4% at a blowing ratio of 0.6. In contrast, the prediction deviations in the literature models were 16.1% and 8%, respectively. Furthermore, the introduction of the equivalent blowing ratio reduced the data requirements for calculating the single-hole-row cooling efficiency when performing cooling efficiency superposition predictions.

**Keywords:** turbine outer ring; film superposition; mainstream temperature correction; energy conservation in film injection; equivalent blowing ratio

check for updates

Academic Editor: Krzysztof Rogowski

Received: 17 November 2024
Revised: 27 December 2024
Accepted: 2 January 2025
Published: 7 January 2025

**Citation:** Gao, Z.; Qiu, T.; Liu, P.; Ding, S.; Li, Z.; Cheng, R.; Yuan, Q. A Study on the Film Superposition Method for the Multi-Row Film Cooling of the Turbine Outer Ring. *Processes* **2025**, *13*, 143. https://doi.org/10.3390/pr13010143

**Copyright:** © 2025 by the authors. Licensee MDPI, Basel, Switzerland. This article is an open access article distributed under the terms and conditions of the Creative Commons Attribution (CC BY) license (https://creativecommons.org/licenses/by/4.0/).

## 1. Introduction

Increasing the turbine inlet temperature is a key strategy for enhancing engine efficiency. Future turbine inlet temperatures are expected to reach 2200 K [1], significantly

exceeding the temperature tolerance of high-temperature alloy materials [2]. Film cooling is one of the key techniques for preventing the overheating of hot-end components. It forms a low-temperature film between the hot gas and the wall, effectively reducing heat transfer and thus controlling the wall temperature [3,4]. Film cooling is essential for ensuring the thermal protection of critical areas, including the leading edge of turbine blades [5], the suction surface of turbine blades [6], the pressure surface of turbine blades [7], the blade endwall [8], the combustion chamber liner [9], and the turbine outer ring [10], ensuring that the materials remain within safe temperature limits.

The turbine outer ring is located outside the turbine blades within the casing and forms the working passage for the turbine blades through a circumferential segmented structure. A typical turbine outer ring structure is shown in Figure 1 [11]. To ensure the safety of the turbine blade tips, a wear-resistant coating is often applied to the outer ring wall to reduce blade damage during rubbing. This results in the thickness of the film cooling hole plates in the turbine outer ring being greater than that of other components, such as the blades. Additionally, the relatively low thermal conductivity of the coating hinders the transfer of internal cooling effects to the hot side wall, making film cooling in the turbine outer ring even more critical compared to other components.

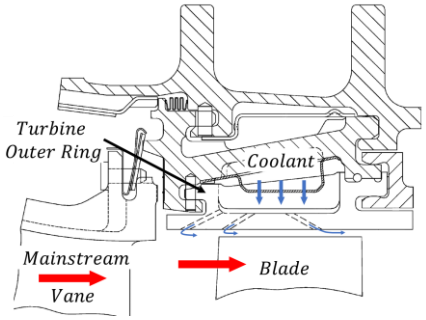



**Figure 1.** Schematic diagram of a typical turbine outer ring structure.

During engine operation, due to the approximately 70° angle between the guide vane exit and the engine axis, the length traversed by the film as it exits the turbine outer ring's front edge is about three times the axial length of the turbine outer ring, significantly increasing the number of hole rows through which the film flows. Additionally, the rotational motion of the turbine blades causes considerable temperature variation along the flow direction on the hot side wall of the turbine outer ring. As the demand for precise cooling increases, the coolant temperature at the turbine outer ring's film hole exits also changes with the position relative to the mainstream airflow. This results in unique challenges during the design of turbine outer ring film cooling: a large number of hole rows, significant variations in the streamwise mainstream and coolant temperatures, and considerable variation in the film hole diameter during the initial design iterations.

During the initial design phase of turbine outer ring components, relying solely on high-dimensional numerical simulations presents challenges, including high computational costs, prolonged design cycles, and difficulties in implementing modifications. These issues become even more pronounced when the turbine outer ring structure is complex and incorporates a large number of film cooling holes. This complexity leads to a rapid increase in the mesh count, significantly extending the design process and resulting in a waste of valuable resources during the early design phase.

To achieve a rapid design, Cui et al. [12] used a data-driven approach combined with decoupled conjugate heat transfer analysis to predict the film cooling efficiency on the surface of the E3 turbine's first-stage blades using Sellers' superposition model. This method avoided complex fluid simulations and reduced the iteration time. It provides a

good approach for the initial design of the turbine outer ring. The accurate prediction of the film cooling efficiency is key to ensuring efficient design iterations.

Sellers' superposition formula [13] is the most widely used model for predicting film cooling. Many studies have validated the Sellers model. Muska et al. [14] first tested its use for predicting the film cooling efficiency on turbine blades. They found it could predict the cooling efficiency well. Mhetras et al. [15,16] also confirmed its high applicability in turbine blade studies. Wang et al. [17] showed that the Sellers model is adaptable to mixed cooling methods, including slot film cooling and film hole cooling.

However, although Sellers' superposition model has shown good prediction accuracy in many applications, its applicability and accuracy are still uncertain under different operating conditions, especially in complex geometries and flow conditions.

This is mainly because the Sellers model cannot account for the diffusion of the film in the streamwise direction and the interaction between adjacent rows of film holes during the superposition process. These effects are mainly influenced by the blowing ratio and hole spacing.

The blowing ratio of the film is the most significant factor affecting the prediction accuracy. In flat plate film cooling predictions, Sasaki et al. [18] showed that the Sellers model can effectively predict the cooling performance at lower blowing ratios but tends to overestimate the results at slightly higher blowing ratios. Meng et al. [19] confirmed this conclusion in their study on two rows of holes.

In blade studies, the Sellers model also demonstrated good prediction accuracy at low blowing ratios, but the prediction accuracy varied at different positions on the blade. Li et al. [20,21] found that the prediction accuracy of the Sellers superposition model for the blade leading edge was similar to that for flat plates. They suggested that the poor prediction performance at high blowing ratios is due to the strong interaction between the mainstream and secondary flows, as well as the vortex between hole rows, which weakens the model's accuracy. Anderson et al. [22] found that for the blade suction side, the model accurately predicted film cooling at low blowing ratios but underestimated the cooling at high blowing ratios. Takeishi et al. [23] found that the Sellers model provided more reasonable predictions for the turbine blade pressure side, but the predictions for the suction side were about 30% lower than the experimental values.

The variation in hole spacing also affects the accuracy of the Sellers superposition model. Sasaki et al. [18], while studying the influence of the blowing ratio, also examined the effect of hole row spacing. Their results showed that reducing the hole spacing decreases the prediction accuracy of the Sellers model. Wang et al. [24] reached the same conclusion in their study on two rows of holes, finding minimal errors when the $S/D$ was 20. Meng et al. [19] further reduced the critical value of hole spacing and concluded that when the spacing reaches 5d, the Sellers model achieves better accuracy. Murray et al. [25] suggested that at smaller hole spacings, higher film interactions occur between the holes, which reduces the accuracy of the superposition method. In their study of double hole rows, Huo et al. [26] found that at a blowing ratio of 1.25 and a hole spacing of 5D, the maximum error reached 65%.

The impact of staggered versus inline hole arrangements on the accuracy of prediction models is similar to that of hole spacing. For the same hole row spacing, the hole spacing along the streamwise direction in a staggered arrangement is twice that of an inline arrangement. Based on the effect of hole spacing, the prediction accuracy for staggered arrangements should be superior to that of inline hole arrangements. Chen et al. [27] used the 2D Sellers superposition model to evaluate the performance of fan-shaped holes with different hole row spacings. The results showed that the prediction model matched well with the staggered arrangement at a spacing ratio of one but overestimated the cooling

efficiency of the inline holes. Liu et al. [28] used the Sellers superposition model to evaluate the film cooling efficiency of two rows of holes under cross-flow conditions. Their results showed that the model had good applicability when the holes were staggered and at lower blowing ratios, with errors within 8%. However, under inline arrangements and high blowing ratios, the model performed poorly, with prediction errors exceeding 10%.

Research on the blowing ratio of film cooling holes and hole row spacing indicates that the main cause of deviation in the Sellers superposition model is its insufficient consideration of the interaction between the film outflow and the mainstream during the film superposition process. Boundary parameters, such as the mainstream turbulence intensity (Ethridge et al. [29,30]), which affect film mixing also directly impact the accuracy of the Sellers model.

In the future design of turbine outer rings, full film cooling will be a necessary method. Most of the studies mentioned above have focused on the superposition effect of two rows of film cooling holes, but Li et al. [31] argue that due to increased mixing and turbulence, the Sellers superposition model is unreliable when predicting film cooling for multi-row structures, especially for full film cooling configurations. Therefore, research to improve the Sellers superposition model is necessary to support the prediction of the film cooling efficiency for turbine outer rings.

Currently, improvements to the Sellers superposition model can be broadly classified into four categories.

The first category of model improvement methods suggests that, during the film superposition process, the coverage effect of a single film stops once it reaches a critical position due to the interaction between the films. This effectively reduces the overestimation of the film cooling efficiency. Andreini et al. [32] adjusted the superposition length for different hole row configurations, enabling the Sellers superposition model to accurately predict the average cooling efficiency for both inline and staggered nine-row film hole arrangements. The superposition length for staggered holes was consistently higher than that for inline holes, with the length ranging from two to five. Later, Wang et al. [33] examined the superposition characteristics of full film cooling with five rows of staggered holes. By adding a critical number of film hole rows to the Sellers superposition model, they reduced the prediction deviation for multi-row film cooling configurations.

The second category of models is essentially an extension of the Sellers model, applying the commonly used one-dimensional superposition model to two-dimensional models. The aim is to address the accuracy issues in the prediction of inline and staggered hole configurations. Murray et al. [25], Chen et al., 2020 [27], and Chen et al., 2021 [34] all employed the two-dimensional Sellers model to predict film cooling for two rows of holes. This primarily expanded the capability to capture the cooling efficiency distribution; however, there was no significant improvement in accuracy when considering the spanwise average cooling efficiency.

The third category of models assumes that the interaction between film holes during the film cooling process leads to changes in the local cooling efficiency of downstream film holes. By introducing a correction factor, the cooling efficiency of the downstream film can be adjusted, either reducing or amplifying the impact of film cooling in the prediction process. Zhang et al. [35] proposed a new superposition formula for predicting the two-hole-row model under different operating conditions, using $M$ as an unknown variable. This method greatly improved the accuracy of cooling efficiency predictions. However, this approach is not widely applicable. To address this, scholars established a general form: $\eta = \eta_1 + \eta_2 - C\eta_1\eta_2$, where C is adjusted to modify the predicted cooling efficiency. Xu et al. [36] suggested that the correction factor for turbine blades depends on both the blowing ratio, M, and the dimensionless distance, $X/D$. They established a

fitting relationship between these factors to correct the predicted cooling efficiency of the blade film. Huo et al. [26] further incorporated the dimensionless hole pitch in their study of mist-assisted film cooling on flat surfaces. However, applying this to full film cooling makes obtaining the correction factor for the Sellers model under full film cooling extremely challenging, as it requires significant computational effort. Zhang et al. [37] eliminated the effect of dimensionless distance in the model correction, stating that the correction factor is only related to the number of hole rows and the Reynolds number of the film holes. By adjusting the correction factor for different hole rows, they significantly reduced the prediction deviation. Zhang et al. [38] examined the cooling efficiency superposition problem for film holes with more than 50 rows. They proposed that the correction factor for the superposition model is related to the spanwise non-uniformity factor and the streamwise dissipation rate. Through extensive numerical simulations, they established a correlation, and the predicted results showed good agreement with experimental data.

The fourth category of calibration models is based on energy conservation. The essence of film cooling lies in the impact of the mixing ratio between the coolant and mainstream on the wall temperature. The film superposition process continuously adjusts this mixing ratio, thereby altering the adiabatic wall temperature distribution. Kirollos et al. [39] proposed an energy conservation-based superposition method for multi-row cooling holes. An et al. [40] found that the influence of the upstream flow on downstream cooling is reflected in changes in the turbulence intensity. The increase in turbulence negatively impacts the cooling efficiency of the downstream film, particularly in regions further downstream. They introduced a correction factor, $\beta$, to evaluate the impact of coolant jetting on mainstream entrainment from the upstream row.

Table 1 summarizes the existing correction models for the film superposition. In the initial design of turbine outer rings, there are several challenges due to the large number of cooling holes, significant variations in the streamwise mainstream and coolant temperatures, and considerable changes in the film hole diameter during the design iterations. The first category of correction models requires the continuous adjustment of the critical hole row number at different hole row positions, which presents a significant challenge in the initial design of the outer ring. The second category involves the dimensional expansion of the model; however, it has not resulted in noticeable improvements in the prediction accuracy. The third category of models provides promising results for the superposition of film cooling in cases with large hole numbers, but it lacks a consideration of streamwise temperature variations and requires extensive databases to handle continuous changes in the hole diameter, making it difficult to rapidly iterate the film cooling predictions for the outer ring. The fourth category of correction models, based on energy conservation assumptions, breaks through the independence assumption between film layers and considers the interactions and energy exchange between the layers. This approach provides a solid foundation for the study of film superposition models for turbine outer rings. However, current research is limited to two rows of holes and does not yet account for streamwise temperature variations or the need for a rapid superposition process.

In summary, existing film superposition models are not well suited to evaluating the film superposition for advanced cooling methods in the future design of turbine outer rings. Therefore, new research is necessary. This paper proposes a novel film superposition model that, by incorporating energy conservation, accounts for the interaction between film layers during the superposition process. The model also integrates a dimensionless temperature coefficient to consider the variations in the streamwise coolant and mainstream temperatures, effectively addressing the film cooling prediction issues for turbine outer rings.

To tackle the challenge of large variations in the film hole diameter during the initial design, which leads to substantial data requirements, the concept of an equivalent blowing ratio was introduced. By predicting the streamwise cooling efficiency distribution under fixed spanwise hole spacing, the model can estimate the streamwise cooling efficiency for different hole spacings, thereby reducing the need for extensive databases on the single-row film cooling efficiency.

**Table 1.** Existing correction models for film superposition.

| Category Number | Reference | Superposed Model Equation | Remark |
|---|---|---|---|
| 1 | Andreini et al. [32]<br>Wang et al. [33] | $\eta_{n_all}(x) = 1 - \prod_{i=1}^{n}[1-\eta_i(x)]$,<br>$1-\eta_{n_all}(x) = [1-\eta_{c_all}(x)]\prod_{i=c+1}^{n}[1-\eta_i(x)]$, | "$c$" is a critical row in full-coverage film cooling, and after this row, the film cooling efficiency for an extra row would not change. |
| 2 | Murray et al. [25]<br>Chen et al. [27]<br>Chen et al. [34] | $\eta(x,y) = 1 - \prod_{i=1}^{n}[1-\eta_i(x,y)]$, | The original one-dimensional Sellers superposition model is extended to a two-dimensional model. |
| 3 | Zhang et al. [35] | $\eta = \eta_1 \times M^{5.63} + \eta_2 \times M^{-2.44} - 0.13 \times \eta_1 \times (1-\eta_2) \times M^{9.16}$, | |
| | Xu et al. [36] | $\eta = \eta_1 + \eta_2 - C\eta_1\eta_2$, | $C = f\left(M, \frac{X}{D}\right)$, |
| | Huo et al. [26] | | $C = f\left(M, \frac{S}{D}, \frac{X}{D}, \frac{m_d}{m_c}, \frac{d_d}{D}\right)$. |
| | Zhang et al. [37] | $\eta = 1 - \prod_{i=1}^{n}(1-Z_i\eta_i)$, | $Z_i = f(N, Re_d)$. |
| | Zhang et al. [38] | $\eta = 1-(1-\eta_1)(1-(1-c_1\alpha_1-c_2\beta_2)\eta_2)*\cdots*(1-(1-c_1\alpha_n-c_2\beta_n)\eta_n)$, | $\beta_n = f(n,\ s/p)$,<br>$c_1 = f(M, \frac{p}{D}, \frac{s}{D}, \theta)$,<br>$c_2 = f(M,\ p/D, s/D,\ \theta)$,<br>$\alpha_1$ is the non-uniformity of the gas film flow direction. |
| 4 | Kirollos et al. [39] | $T_{0n}(X) = \frac{T_c\dot{m}_{cn} + \int_{X_n-\delta x}^{X} T_{0(n-1)}(x)\frac{d\dot{m}_{en}(x)}{dx}dx}{\dot{m}_{cn}+\dot{m}_{ei}(X)}$,<br>$T_w(X) = \begin{cases} T_{0i}(X), i = 1,2,\cdots,n-1,\ x_i \le X \le x_{i+1} \\ T_{0n}(X), X \ge x_n \end{cases}$, | |
| | An et al. [40] | $\eta = 1-(1-\frac{\eta_1}{1-(1-\beta)(1-\eta_1)})(1-\eta_{2,a})$, | $\beta = \frac{\chi_j}{\chi_j+\chi_1+1}, \chi_j = \frac{1}{\eta_j} - 1,\ \chi_1 = \frac{m_{e,1}}{m_c}$. |

An adiabatic film cooling efficiency test rig was developed. By comparing the predicted adiabatic film cooling efficiency for different hole arrangements, the applicability of the new film superposition model was confirmed. Compared to existing models, it showed superior predictive performance within a certain range. The introduction of this model provides valuable insights for predicting films in complex cooling structures and can effectively support the initial design of such structures.

## 2. Film Superposition Method

### *2.1. Sellers Superposition Model*

This section reviews the basic principles of the Sellers film superposition model [13], with the core assumptions as follows:

1. The coolant films generated by different rows of holes are independent of each other. Specifically, when coolant is injected through the film holes, the gasses ejected from each row of holes form independent film layers.
2. The adiabatic cooling efficiency at a given location is the combined effect of the adiabatic cooling efficiency of all upstream film holes.

Based on the above assumptions, when the number of hole rows is $n$, the adiabatic cooling efficiency at the wall can be expressed by Equation (1).

$$\eta = \eta_1 + \sum_{i=2}^{n} \eta_i \prod_{j=1}^{i-1} (1 - \eta_j), \tag{1}$$

where $\eta_i$ and $\eta_j$ are the local adiabatic film cooling efficiencies created by the $i$-th and $j$-th row (with $j < i$), meaning the $j$-th row is upstream of the $i$-th row. $n$ is the total number of hole rows. This equation expresses the total cooling efficiency ($\eta$) as the combined effect of the individual cooling efficiencies from each row of holes. The product term $\prod_{j=1}^{i-1}(1 - \eta_j)$ explains the influence of upstream film holes on downstream film holes.

The adiabatic film cooling efficiency of the $i$-th row of holes can be represented by Equation (2).

$$\eta_i = \frac{T_g - T_{aw,i}}{T_g - T_c}, \tag{2}$$

As shown in Figure 2, as the number of hole rows increases, the deviation caused by the independence assumption in the Sellers model accumulates, leading to significant discrepancies between the predicted and actual cooling efficiency results. Therefore, the film cooling efficiency superposition prediction model must consider the interaction between the film injection and the mainstream flow to mitigate the predictive bias introduced by the Sellers independence assumption.

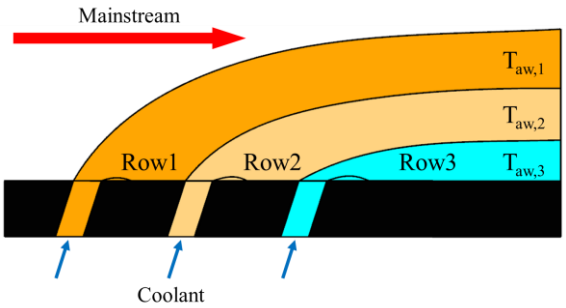



**Figure 2.** Schematic of Sellers superposition model.

### *2.2. Energy Conservation-Based Prediction Method for Multi-Row Film Cooling of Turbine Outer Ring*

To overcome the independence assumption between film hole rows in the Sellers model and support the prediction of the film cooling efficiency for the turbine outer ring, this model proposes the following assumptions:

1. The mixing process between the coolant film and the mainstream flow follows the principle of energy conservation. Previous studies (Kirollos et al. [39]) have demonstrated the validity of this method for two hole rows.
2. The interaction between the film layers is confined to a small region during film injection. In the study by Berkache et al. [41], it was observed that at a blowing ratio

of 1, the velocity of the coolant film in the normal direction toward the wall rapidly mixes with that of the mainstream flow, supporting this assumption.

3. The equivalent blowing ratio is used to evaluate the cooling efficiency distribution for different hole spacings based on the reference cooling efficiency distribution. This assumption extends the applicability demonstrated by Bogard et al. [42] for slot film cooling.

Therefore, the process of film superposition can be described as follows.

The injection from downstream film holes causes a sudden increase in the boundary layer thickness, and a portion of the mainstream flow enters the boundary layer. This impacts the mainstream temperature during film injection, resulting in variations in the cooling efficiency.

As shown in Figure 3, when the coolant flow is injected, the boundary layer thickness experiences a sudden increase. If the coolant mass flow rate is $m_c$, an excess thin layer with a mass flow rate of $C_1 m_c$ is generated. At this point, the mass flow rate of the mainstream entering the boundary layer is $C_2 m_g$. Based on the principles of energy conservation, the mainstream temperature at the downstream row of holes can be determined, as shown in Equation (3).

$$(C_1 m_c + C_2 m_g) T'_{aw} = C_1 m_c T_{aw} + C_2 m_g T_g, \tag{3}$$

where $T'_{aw}$ represents the temperature after mixing. Harrington et al. [43] argued that a superposition model based on the single-row film cooling efficiency distribution tends to overestimate the overall film cooling efficiency. Therefore, the empirical coefficients $C_1$ and $C_2$ are both positive values.

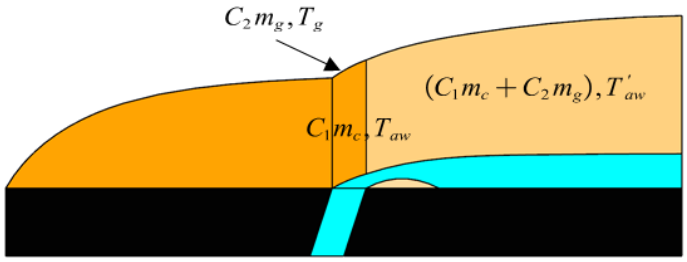



**Figure 3.** Effect of cooling air injection on mainstream temperature.

When film injection occurs, the upstream film cooling efficiency is affected, leading to a slight increase in the heat transfer temperature. After non-dimensionalization, Equation (4) is obtained.

$$\frac{T_g - T'_{aw}}{T_g - T_{aw}} = \frac{C\frac{m_c}{m_g}}{C\frac{m_c}{m_g} + 1}, \tag{4}$$

Equation (4) indicates that when the coolant injection rate is low, the mixing effect of the mainstream flow is slightly enhanced, leading to a higher wall temperature.

This study introduced the mainstream temperature correction factor, $\alpha_i$, to quantify the degree of mixing of the mainstream temperature at varying coolant injection rates, as expressed in Equation (5).

$$\alpha_i = \frac{a\frac{m_i}{m_g}}{a\frac{m_i}{m_g} + 1} + b, \tag{5}$$

where $a$ and $b$ are empirical coefficients and $\frac{m_i}{m_g}$ represents the ratio of the coolant mass flow rate to the mainstream mass flow rate for the $i$-th row of holes.

The mainstream temperature experienced by the film holes from the $i$-th row to the subsequent row is given by Equation (6).

$$T'_{aw,i} = T_{g,i} - \alpha_i \left( T_{g,i} - T_{aw,i} \right), \tag{6}$$

where the subscript $i$ denotes the $i$-th row of film holes and $T_{g,i}$, $T_{aw,i}$, $\alpha_i$, and $T'_{aw,i}$ correspond to the mainstream temperature, the adiabatic wall temperature generated by the film cooling, the mainstream temperature correction factor, and the mixed mainstream temperature at the position of the $i$-th row of film holes, respectively.

After incorporating the correction for the mainstream temperature, the film cooling superposition model becomes Equation (7). This model captures the cumulative effect of film cooling across multiple rows of film holes, where the cooling efficiency of each row is influenced by both the local temperature and the interactions with other rows.

$$\eta = \sum_{i=1}^{n} \left[ \eta_i \prod_{j=i}^{n-1} \alpha_j \prod_{k=i+1}^{n} (1 - \eta_k) \right], \tag{7}$$

where $\eta_i$ represents the adiabatic cooling efficiency for the $i$-th row of film holes. $\alpha_j$ is the mainstream temperature correction factor for the $j$-th row of holes, acounting for the mixing effect between the mainstream and coolant temperatures.

During the iterative design process of the turbine outer ring, variations in the hole spacing and diameter, driven by constraints on the minimum hole diameter and changes in flow rates between different hole rows, increase the demand for a database of single-hole-row film cooling efficiencies. Bogard et al. [42] analyzed the spanwise-averaged film cooling efficiency along the streamwise direction as a function of $X/Ms$ for various hole spacings, as shown in Equation (8). The results indicated that, within the tested range, the trends in the cooling efficiency were largely consistent across different spacings. This finding suggests an effective approach: structures with varying hole spacings can be equivalently represented by a baseline configuration, enabling the cooling efficiency for any specific spacing to be derived from the baseline distribution.

$$\eta = f\left( \frac{X}{Ms} \right), \tag{8}$$

where $X$ represents the distance from the origin along the streamwise direction, $M$ represents the blowing ratio of the film, and s represents the width of the film cooling slot. An equivalent slot width, $s$, is defined as shown in Equation (9).

$$s = \frac{A_{hole}}{P}, \tag{9}$$

where $A_{hole}$ represents the area of each individual hole and $P$ denotes the pitch of holes (the distance between the centers of adjacent holes).

Therefore, an equivalent blowing ratio, $M_e$, is used to normalize the number of holes and their spacing to the baseline single-hole-row cooling configuration. The assumptions for the equivalent blowing ratio are shown in Equation (10).

$$M_e = M_0 \frac{A_0}{A_e}, \tag{10}$$

where $M_0$ and $M_e$ are the blowing ratios for the initial and equivalent hole configurations, respectively. $A_0$ and $A_e$ represent the areas of the initial and equivalent configurations.

During the design process of the turbine outer ring, the mainstream temperature and cooling temperature vary at different locations. Using a fixed temperature can lead to significant discrepancies in the predicted cooling efficiency. When the mainstream and cooling temperatures change, $\xi_{g,i}$ and $\xi_{c,i}$ are used to represent the dimensionless results

at different positions. Therefore, the adiabatic cooling efficiency for $n$ rows of film holes should be expressed as Equation (11).

$$\eta = \sum_{i=1}^{n} \left\{ [\xi_{g,i}(1-\alpha_{i-1,i>1})(1-\eta_i) + \xi_{c,i}\eta_i] \prod_{j=i}^{n-1} \alpha_j \prod_{k=i+1}^{n} (1-\eta_k) \right\}, \quad (11)$$

where $\xi_{c,i} = \frac{T_{g,max}-T_{c,i}}{T_{g,max}-T_{c,min}}$ and $\xi_{g,i} = \frac{T_{g,max}-T_{g,i}}{T_{g,max}-T_{c,min}}$ represent the dimensionless coolant and mainstream temperatures at the $i$-th row of holes, respectively. $T_{c,min}$ denotes the minimum coolant temperature, which is lower than the local coolant temperature at each row of film holes. $T_{g,max}$ represents the maximum mainstream temperature, which is higher than the mainstream temperature at each film hole location.

## 3. Experimental Method

### *3.1. Experimental System*

The experimental system, as illustrated in Figure 4, consisted of two primary flow paths: the mainstream for simulating high-temperature airflow and the coolant for film cooling. Prior to entering the test chamber, both flows passed through a honeycomb structure and a damping mesh to ensure uniformity. A pressure stabilization chamber was also installed at the coolant inlet to further minimize non-uniformities. The mainstream channel had a height of 120 mm and a width of 110 mm, with the first row of film cooling holes located 660 mm downstream from the mainstream inlet.

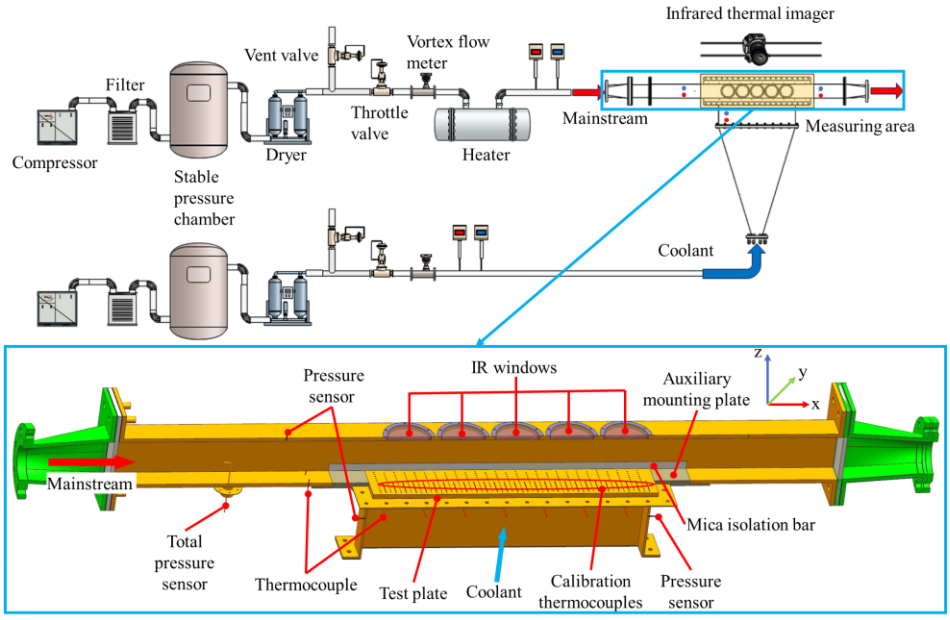



**Figure 4.** Experimental system schematic.

During the experiment, the mainstream mass flow rate, temperature, and coolant mass flow rate were precisely controlled by adjusting the throttle valves, vent valves, and heater power, enabling the accurate regulation of various test conditions. The surface temperature distribution of the test plate was measured using an infrared thermal imaging camera and thermocouples.

### *3.2. Experimental Measurement Methods*

The experiment measured the airflow velocity at the mainstream inlet and outlet using total pressure, static pressure, and temperature sensors. Static pressure sensors were arranged along the test plate to monitor variations in the mainstream static pressure. Multiple pressure and temperature sensors were installed in the cooling air stabilization

chamber to ensure the uniformity of the inlet boundary. The flow rates of both the cooling air and mainstream gas were regulated using mass flow meters.

The coolant mass flow rate was measured using an $FLVJ-KJM12A040-16A1Y2T2$ vortex flowmeter with a measurement error of $\pm 1\%$. The average mass flux through the film holes, $\rho_c u_c$, was obtained using $m_c / A_c$. The mainstream mass flow rate was measured with an $ISA1932$ standard orifice plate, also with a measurement error of $\pm 1\%$. The average mass flux through the mainstream channel, $\rho_g u_g$, was calculated using $m_g / A_g$. Subsequently, the blowing ratio, $M$, during the experiment was determined using $\rho_c u_c / \rho_g u_g$.

The mainstream temperature, $T_g$, was measured by three $K-type$ total temperature thermocouples located 186 mm upstream of the film cooling hole plate. The coolant temperature was measured by seven $K-type$ total temperature thermocouples uniformly arranged along the wall of the coolant chamber, with a measurement deviation of $\pm 0.75\%$.

The wall temperature of the test plate was obtained using two methods:

1. A total of 27 wall thermocouples were evenly distributed along the centerline of the mainstream-side wall of the test plate to measure the centerline wall temperature $T_{aw}$. The measurement deviation for these thermocouples was $\pm 0.75\%$, and they were also used to calibrate the results from the infrared thermal imaging system.
2. The surface temperature distribution of the mainstream-side wall was obtained using the $Filr\ SC$ 620 infrared thermal imaging system, which operates within a wavelength range of 7.5 μm to 13 μm, with a resolution of $640 \times 480$ pixels and an accuracy of $\pm 1$ K. To ensure precise temperature readings, five circular $ZnS$ infrared windows were installed at corresponding positions on the test plate, providing excellent image transmission in the wavelength range of 8 μm to 12 μm. Additionally, the mainstream-side wall was coated with black paint to enhance surface emissivity. Taking the position of the first row of film holes as the origin, the streamwise positions for different windows are shown in Table 2.

**Table 2.** Streamwise positions, $X$, for different windows.

| Window Number, $n$ | Upstream $X$ (mm) | Downstream $X$ (mm) |
|---|---|---|
| 1 | 25 | 88 |
| 2 | 162 | 225 |
| 3 | 298 | 361 |
| 4 | 433 | 496 |
| 5 | 569 | 632 |

The infrared camera was positioned directly opposite the test plate. Due to the difficulty of capturing a wide field of view under high-resolution conditions, an electric sliding rail was installed beneath the infrared camera, parallel to the mainstream cavity, allowing the camera to move along the direction of the hot air flow. This setup ensured that each infrared window could be imaged under consistent operating conditions, as illustrated in Figure 5.

Based on the mainstream-side wall temperature measured by thermocouples and the infrared thermal imaging system, the adiabatic film cooling efficiency $\eta$ at the centerline of the mainstream-side wall and the $\eta$ distribution at the infrared window positions could be determined using $\frac{T_g - T_{aw}}{T_g - T_c}$.

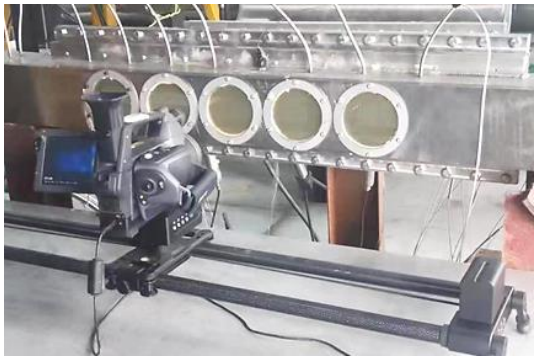


**Figure 5.** Infrared camera capturing on an electric sliding rail.

### *3.3. Design of Test Plates*

The experimental setup included four test plates: one for calibrating the empirical coefficients in the mainstream temperature correction model and three for model validation. Figure 6 illustrates the structure of the test plates, where the streamwise hole spacing is defined as $S$, the spanwise hole spacing as $P$, and the film hole diameter as $d$. Table 3 provides the structural parameters for the different test plates. In *Case* 1 and *Case* 2, the hole spacing ratios $P/d$ and $S/d$ were kept consistent, while the hole diameters were varied to investigate the effect of the hole size on the film cooling efficiency within a fixed cooling area. This design aimed to eliminate the influence of non-geometric factors, such as the blowing ratio, and to explore the impact of hole size variation on the film superposition process.

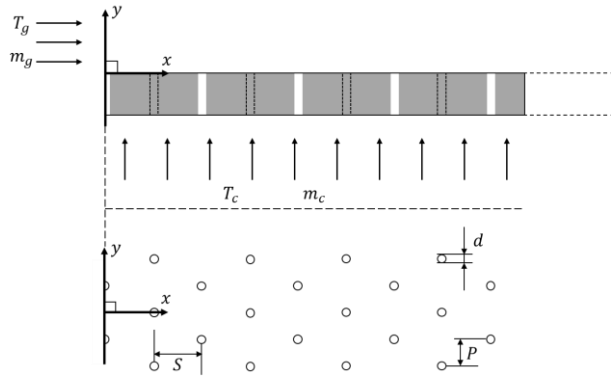



**Figure 6.** Structure of test plates.

**Table 3.** Structural parameters of test plates.

| | ***d* (mm)** | ***L*×*W*×*H* (mm)** | ***P*/*d*** | ***S*/*d*** |
|---|---|---|---|---|
| *Case* 1 | 1.2 | 710 × 110 × 17 | 3.5 | 10.5 |
| *Case* 2 | 1.8 | | 4.7 | 14 |
| *Case* 3 | 2.4 | | 3.5 | 10.5 |
| *Case* 4 | 3.0 | | 2.8 | 8.4 |

The test plates were fabricated using photosensitive resin with an extremely low thermal conductivity, approximately 0.1 $W/(m \cdot K)$, using 3D printing technology, providing nearly adiabatic conditions, as shown in Figure 7. To minimize the impact of flow non-uniformity within the cooling air cavity on the exit airflow from the film holes, the thickness of the test plates was set to 17 mm, ensuring an aspect ratio of approximately 5 between the length and diameter of the cooling holes.

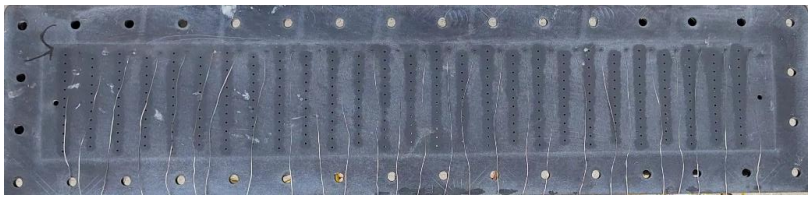


**Figure 7.** Schematic of a 3D-printed test plate.

### *3.4. Experimental Conditions*

In the experiments with different test plates, the same mainstream conditions were maintained. The mainstream inlet temperature was fixed at 360 K, and the inlet mass flow rate was set to 940 g/s to ensure that the mainstream Reynolds number matched the engine operating condition. The mainstream exited to the atmosphere through an 80 mm duct. The cooling air inlet temperature was approximately 300 K. Using *Case* 1 as the baseline, its blowing ratio was set to 0.3, 0.4, 0.5, 0.6, 0.8, and 1.0 during the experiments. For the other test plates, the coolant flow rate was adjusted to match the conditions of *Case* 1. Both the mainstream and coolant used air as the working fluid.

### *3.5. Uncertainty in Experiments*

The infrared temperature distribution results for different test plates were calibrated using thermocouple measurements, as illustrated in Figure 8. Across different test plates, a relatively linear relationship was observed between the infrared data and thermocouple readings, indicating a certain degree of reliability in the results. The calibration formula is provided in Equation (12).

$$T_{TC} = aT_{IR} + b, \tag{12}$$

where $T_{IR}$ is the infrared temperature, $T_{TC}$ is the thermocouple measurement, and $a$ and $b$ are the slope and intercept of the calibration formula, respectively, with a standard error of $\Delta a$ and $\Delta b$. These values can be obtained through linear fitting in Origin 9.1.

Table 4 summarizes the calibration curve parameters of the infrared results based on thermocouple measurements for different test plates.

**Table 4.** Calibration curve parameters for infrared results.

| Test Plate | Slope, $a$ | Intercept, $b$ | Slope Standard Error, $\Delta a$ | Intercept Standard Error, $\Delta b$ |
|---|---|---|---|---|
| *Case* 1 | 1.59201 | −35.2228 | 0.00983 | 0.51673 |
| *Case* 2 | 1.55714 | −32.8684 | 0.02699 | 1.66951 |
| *Case* 3 | 1.57663 | −33.1008 | 0.01902 | 1.00251 |
| *Case* 4 | 1.59836 | −35.0375 | 0.01516 | 0.87287 |

The uncertainty level of the film cooling efficiency was estimated using the partial derivative method proposed by Moffat et al. [44]. In this experiment, the uncertainty of the adiabatic film cooling efficiency, $\Delta\eta$, was calculated using Equation (13).

$$\Delta\eta = \sqrt{\left(\frac{\partial\eta}{\partial T_g}\Delta T_g\right)^2 + \left(\frac{\partial\eta}{\partial T_{aw}}\Delta T_{aw}\right)^2 + \left(\frac{\partial\eta}{\partial T_c}\Delta T_c\right)^2}, \tag{13}$$

where $\Delta T_g$, $\Delta T_c$, and $\Delta T_{aw}$ represent the uncertainties of the mainstream temperature, coolant temperature, and wall temperature, respectively. The partial derivatives $\frac{\partial\eta}{\partial T_g}$, $\frac{\partial\eta}{\partial T_c}$, and $\frac{\partial\eta}{\partial T_{aw}}$ quantify the sensitivity coefficients of how changes in the mainstream temperature, coolant temperature, and wall temperature affect the film cooling efficiency $\eta$. These coefficients can be calculated using Equation (2).

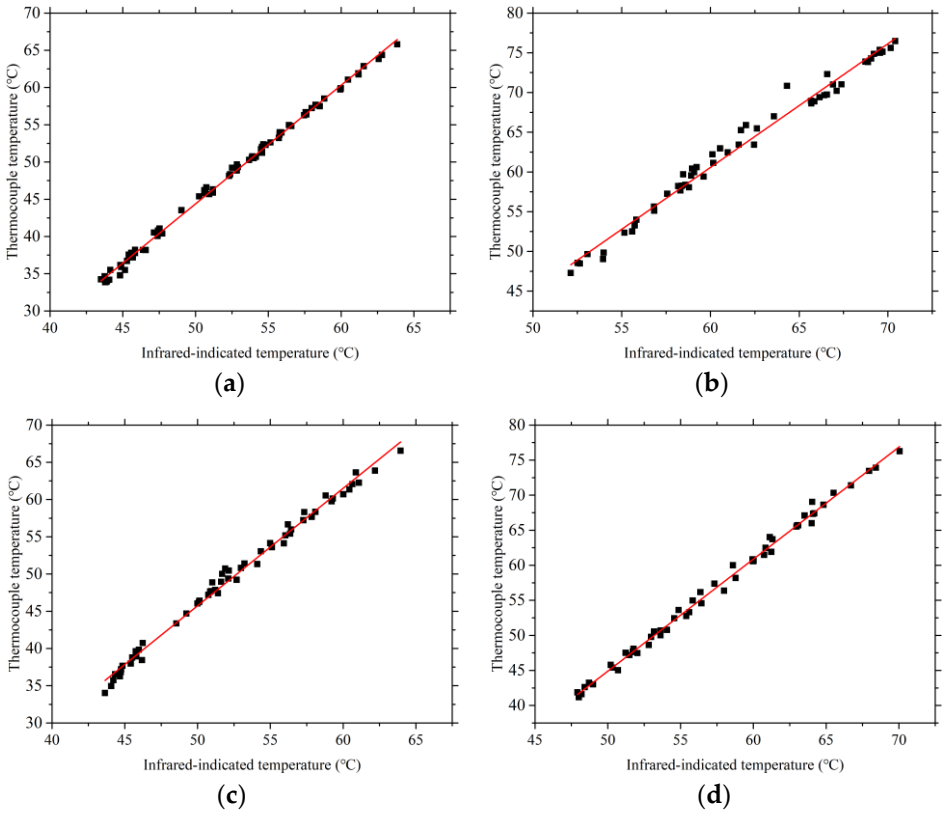



**Figure 8.** Calibration of infrared results for different test plates: (**a**) *Case* 1; (**b**) *Case* 2; (**c**) *Case* 3; (**d**) *Case* 4.

When calculating the cooling efficiency using the temperature obtained from thermocouples, the temperature uncertainty was based on the uncertainty of the thermocouple, $\Delta T_{aw,TC}$. When calculating the cooling efficiency using the temperature obtained from infrared measurements, the uncertainty of the calibrated adiabatic wall temperature, $\Delta T_{aw,IR}$, was determined using Equation (14).

$$\Delta T_{aw,IR} = \sqrt{(a\Delta T_{IR})^{2} + (\Delta a T_{IR})^{2} + (\Delta b)^{2}}, \quad (14)$$

The uncertainty level varied with the adiabatic film cooling efficiency. Figure 9 presents the uncertainty levels of the centerline cooling efficiency and the cooling efficiency distribution for different test plates (with the centerline cooling efficiency derived from thermocouple measurements and the cooling efficiency distribution obtained from calibrated infrared measurements).

The cooling efficiency deviation based on thermocouple measurements was relatively smaller. At an adiabatic cooling efficiency of 0.6, the uncertainty in the cooling efficiency was approximately 0.01. In contrast, the cooling efficiency uncertainty derived from infrared camera measurements ranged from 0.03 to 0.045. When conducting cooling efficiency investigations based on infrared results, a spanwise-averaged cooling efficiency or area-averaged cooling efficiency should be adopted to reduce uncertainty. When the number of pixels is $N$, the testing uncertainty of the infrared cooling efficiency is $\Delta\eta/\sqrt{N}$. Furthermore, the uncertainty in the cooling efficiency decreases consistently as the cooling efficiency level increases.

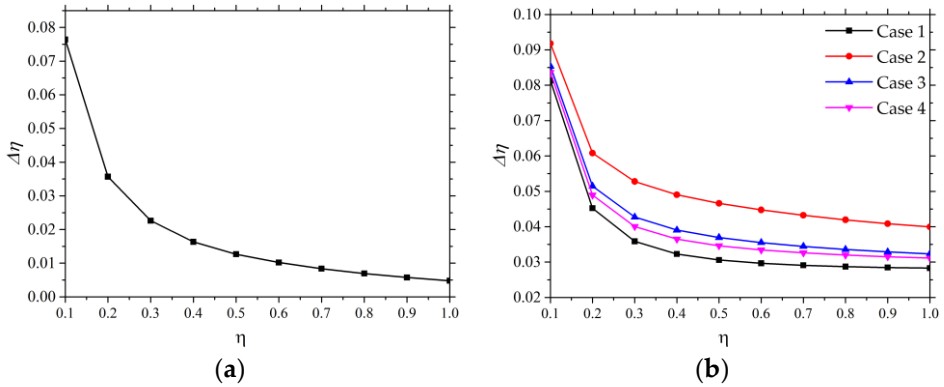



**Figure 9.** Deviations ($\delta\eta$) in experimental cooling efficiency for different measurement methods: (**a**) cooling efficiency ($\eta$) at centerline position obtained from thermocouple measurements; (**b**) cooling efficiency ($\eta$) at infrared window positions derived from infrared camera measurements.

## 4. Results and Discussion

### *4.1. Single-Hole-Row Film Cooling Characteristics*

The distribution pattern of the cooling efficiency for a single hole row serves as the foundation for predicting the superposition effects of film cooling. Based on the experimental results of Eckert et al. [45] regarding the adiabatic cooling efficiency of individual film holes in cylindrical geometries, this study averaged the cooling efficiency data within a 1.5$d$ range from both sides of a single film hole. This yielded the streamwise distribution pattern of the adiabatic cooling efficiency for holes with a spanwise spacing of 3$d$, as shown in Figure 10. Its blowing ratio range was 0.1 to 1.0.

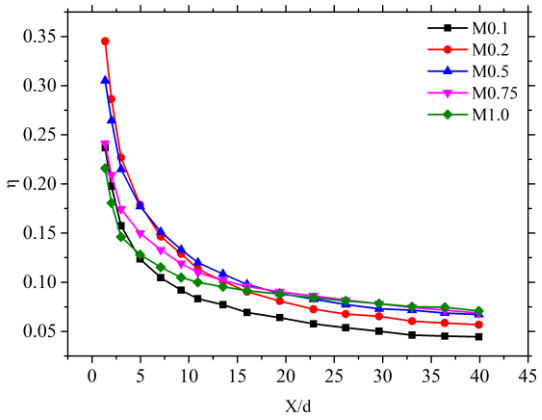



**Figure 10.** Single-hole-row film cooling efficiency ($\eta$) as a function of the non-dimensional streamwise distance ($X/d$) for different blowing ratios ($M$).

### *4.2. Analysis of Sellers Model Predictions for Centerline Adiabatic Film Cooling Efficiency*

Figure 11 illustrates the experimental cooling efficiency results of various test plates and the corresponding cooling efficiency prediction results based on the Sellers superposition model without the equivalent blowing ratio.

In Figure 11a, when the blowing ratios are 0.3 and 0.51, the predicted cooling efficiency consistently exceeds the experimental cooling efficiency. However, at a blowing ratio of 0.8, the predicted cooling efficiency was slightly lower than the experimental efficiency for $X/d < 150$ and then exceeded it as $X/d$ increased. The phenomenon of the experimental cooling efficiency at the leading edge being initially higher and then lower may have been caused by pressure variations along the mainstream channel. Due to flow losses in the mainstream channel, the pressure along the mainstream cavity exhibits a small gradient, whereas the pressure in the coolant supply cavity remains nearly uniform. This pressure

difference causes the coolant flow rate along the streamwise direction to gradually increase, leading to lower experimental efficiency at the leading edge compared to the average blowing ratio. As the blowing ratio increases, the influence of the streamwise pressure gradient on the coolant distribution diminishes, thereby reducing the prediction bias of the model at the leading edge.

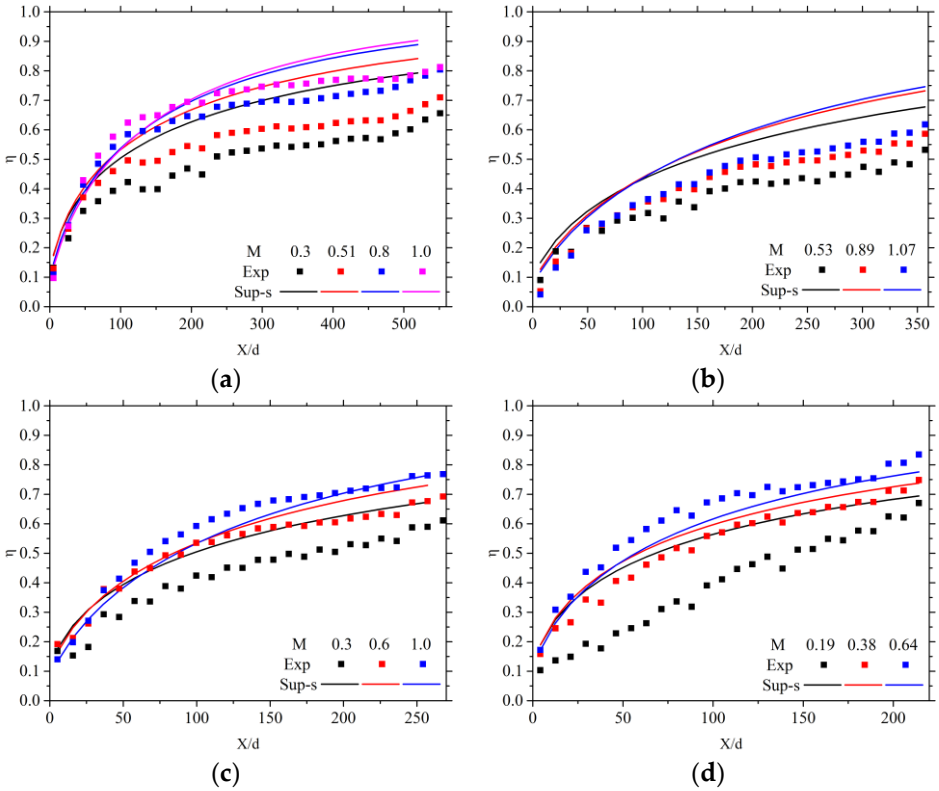



**Figure 11.** Comparison of the Sellers model ($Sup-s$)-predicted cooling efficiency ($\eta$) without the equivalent blowing ratio ($M_e$) and the experimental results ($Exp$) along the non-dimensional streamwise distance ($X/d$) for different test plates at various blowing ratios ($M$): (**a**) *Case* 1 ($d = 1.2$ mm; $P/d = 3.5$; $S/d = 10.5$); (**b**) *Case* 2 ($d = 1.8$ mm; $P/d = 4.7$; $S/d = 14$); (**c**) *Case* 3 ($d = 2.4$ mm; $P/d = 3.5$; $S/d = 10.5$); (**d**) *Case* 4 ($d = 3.0$ mm; $P/d = 2.8$; $S/d = 8.4$).

As $X/d$ increased, the growth rate of the predicted cooling efficiency significantly exceeded that of the experimental efficiency. At a blowing ratio of 0.3, the predicted cooling efficiency was consistently higher than the experimental results. However, as the blowing ratio increased, this phenomenon was alleviated. When the blowing ratio reached one, the difference between the predicted and experimental cooling efficiency became noticeably smaller than at lower blowing ratios. It is evident that, within the range of experimental blowing ratios, the effective area of the predicted cooling efficiency was narrower compared to the experimental cooling efficiency. This variation with the blowing ratio was primarily caused by the independence assumption of the Sellers superposition model. Since the model does not account for interactions between coolant jets or their entrainment effects on the mainstream flow, the superposition error of the Sellers model accumulates as the number of film rows increases, leading to a progressive increase in prediction deviations. However, as the blowing ratio increases, the adhesion of the coolant film to the wall weakens. In the case of full film cooling, the superposition effect mitigates this detachment phenomenon, resulting in an increase in the cooling efficiency. As shown in Figure 10, when the blowing ratio exceeded 0.5, significant film detachment and reattachment occurred, reducing the accuracy of the predictive model. In full film cooling, this detachment phenomenon is delayed, which reduces the gap between the predicted and experimental cooling efficiency

as the blowing ratio increases. In Figure 11c, the streamwise and spanwise hole spacings of the test plate are identical to those in Figure 11a, but the hole diameter is increased from 1.2 mm to 1.4 mm. Dimensionlessly, the distribution patterns of the predicted and experimental cooling efficiency remained essentially the same. However, for a fixed cooling area, the cooling efficiency level at larger hole diameters was significantly lower than that at smaller hole diameters.

Under fixed conditions of $S$ and $P$, *Case* 2, *Case* 3, and *Case* 4 modified the dimensionless hole spacing by varying the film hole diameter; the distribution of the cooling efficiency is shown in Figure 11b, c and d, respectively. *Case* 2 exhibited the largest dimensionless hole spacing, while *Case* 3 featured the smallest. The general relative deviation between the cooling efficiency predicted by the Sellers model and the experimental results decreased progressively as the dimensionless hole spacing reduced. In *Case* 2, the predicted cooling efficiency was consistently higher than the experimental results across various blowing ratios. In contrast, the predicted results in *Case* 3 closely aligned with the experimental results at a blowing ratio of one. In *Case* 4, the predicted cooling efficiency was lower than the experimental results at higher blowing ratios.

This phenomenon is primarily due to the use of a single-hole cooling efficiency distribution model under fixed spanwise hole spacing in the prediction model. For a single film hole, the cooling efficiency decreases as the distance from the centerline increases. The presence of multiple film holes within the row inhibits the lateral spreading of each film, leading to a gradual reduction in the average cooling efficiency as the spanwise hole spacing increases at a fixed blowing ratio.

In *Case* 2, shown in Figure 11b, when $X/d = 100$, an inflection point manifested. Prior to this point, the cooling efficiency with a blowing ratio of 0.53 was the largest, and subsequent to this point, the cooling efficiency with a blowing ratio of 0.53 was the smallest. This is primarily ascribed to the film detachment phenomenon at high blowing ratios. It can be observed in Figure 10 that the film detachment phenomenon initiated when the blowing ratio exceeded 0.5. Although in the full film cooling, the superposition of the films would mitigate this phenomenon, the degree of alleviation for the film detachment phenomenon at the leading edge was relatively small. Hence, at the leading edge, the cooling efficiency with a blowing ratio of 0.53 was the highest. With the superposition of the films, the detached cold gas would reattach to the wall surface once again, which led to a higher rate of increase in the cooling efficiency under a large blowing ratio, resulting in the smallest cooling efficiency when the blowing ratio was $M = 0.53$ and when $X/d > 100$.

Excluding the errors introduced by the Sellers superposition prediction model, the prediction for *Case* 2, with its larger spanwise hole spacing, tended to overestimate the cooling efficiency. As the spanwise hole spacing decreased, the cooling efficiency along the flow direction tended to be underestimated. When combined with the overestimation introduced by the Sellers superposition model, this resulted in the phenomenon observed in Figure 11b–d.

To verify the applicability of the cooling performance characteristics of a single hole row with fixed hole spacing under the assumption of an equivalent blowing ratio, the cooling efficiency was predicted for *Case* 2 and *Case* 4 based on this assumption. The comparison results are shown in Figure 12.

Compared to the cooling efficiency distribution without the equivalent blowing ratio, *Case* 2 demonstrated significant improvement, with the predicted cooling efficiency decreasing and aligning more closely with the experimental results. As the number of hole rows increased, the rate of the cooling efficiency change decreased, resulting in smaller prediction errors compared to cases without the equivalent blowing ratio.

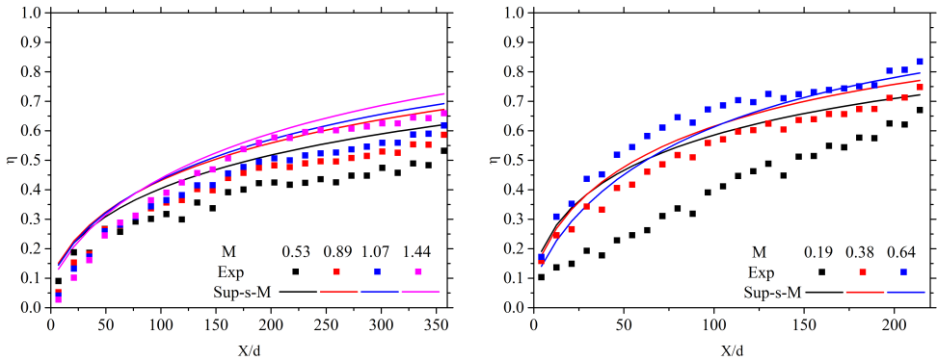



**Figure 12.** Comparison of the Sellers model ($Sup - s - M$)-predicted cooling efficiency ($\eta$) with the equivalent blowing ratio ($M_e$) and the experimental results ($Exp$) along the non-dimensional streamwise distance ($X/d$) for different test plates at various blowing ratios ($M$): (**a**) *Case* 2 ($d = 1.8$ mm; $P/d = 4.7$; $S/d = 14$); (**b**) *Case* 4 ($d = 3.0$ mm; $P/d = 2.8$; $S/d = 8.4$).

Under the equivalent blowing ratio condition, the distribution and efficiency of single-row film holes were predicted more accurately, thereby more realistically reflecting the actual conditions of film cooling and improving the prediction accuracy.

### *4.3. Analysis of Mainstream Temperature Correction Model Predictions*

This section provides an in-depth discussion of the predictive model using various film cooling efficiency indicators. First, the empirical coefficients of the model were calibrated based on the centerline cooling efficiency distribution, and comparisons were made across different hole spacings to better understand the characteristics of mixing, penetration, and wall adhesion between the cooling airflow and the hot mainstream. Next, the spanwise-averaged cooling efficiency, which reflects the film's spreading capability and overall uniformity of coverage, was analyzed to evaluate the model's predictive accuracy in characterizing the cooling efficiency on the wall surface. Finally, the area-averaged cooling efficiency, representing the overall cooling performance of the film on the wall surface, was compared across different locations to assess the model's predictive deviations at various positions and to evaluate its overall cooling performance.

#### 4.3.1. Centerline Cooling Efficiency Prediction

The empirical coefficients in the correction model were calibrated using the cooling efficiency distributions from *Case* 1 at blowing ratios of 0.3 and 1.0. The empirical coefficients in Equation (5), $a$ and $b$, were determined to be 12 and 0.9465, respectively.

Figure 13a shows a comparison between the predicted cooling efficiency based on the mainstream temperature correction model and the experimental cooling efficiency for *Case* 1. It is evident from Figure 13a that the mainstream temperature correction model effectively reduced the overestimation of the cooling efficiency at higher hole row counts under various blowing ratios. Compared to the predictions from the Sellers superposition model, the accuracy of the cooling efficiency predictions was significantly improved. At lower hole row counts, predictions from both models were approximately equivalent, primarily due to the limited adjustments introduced by the mainstream temperature correction model. As the number of hole rows increased, the effects of the mainstream temperature correction became more pronounced, reducing the Sellers model's tendency to overestimate the cooling efficiency and thereby improving the accuracy of streamwise cooling efficiency predictions.

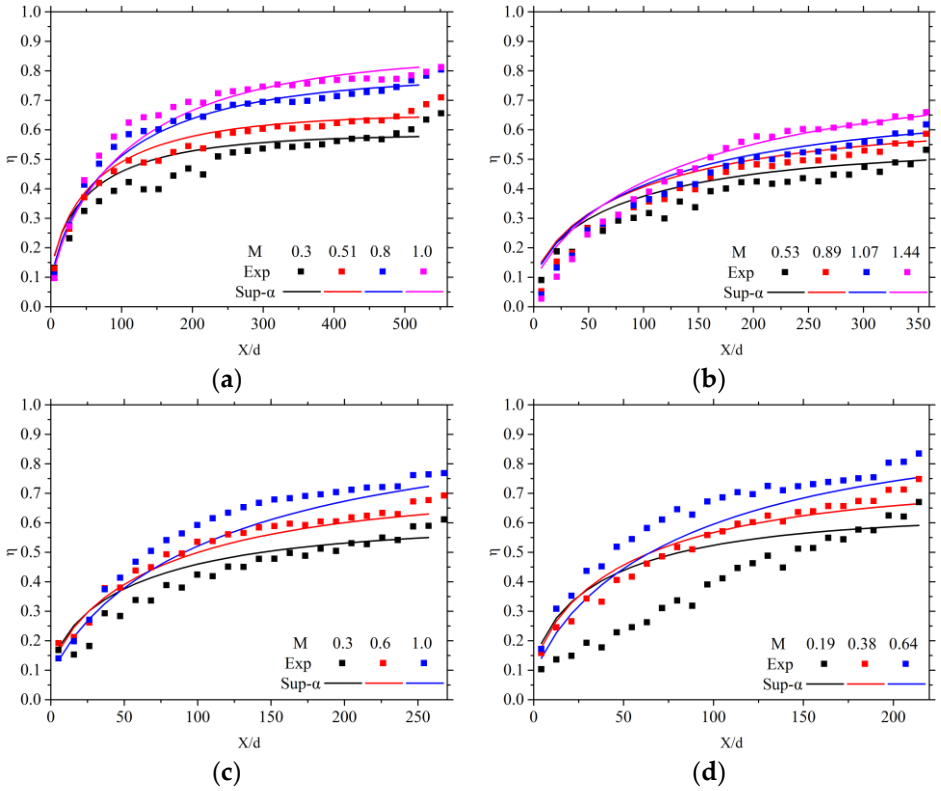



**Figure 13.** Comparison of the superposition model based on the mainstream temperature correction model ($Sup-\alpha$)-predicted cooling efficiency ($\eta$) and the experimental results ($Exp$) along the non-dimensional streamwise distance ($X/d$) for different test plates at various blowing ratios ($M$): (**a**) *Case* 1 ($d = 1.2$ mm; $P/d = 3.5$; $S/d = 10.5$); (**b**) *Case* 2 ($d = 1.8$ mm; $P/d = 4.7$; $S/d = 14$); (**c**) *Case* 3 ($d = 2.4$ mm; $P/d = 3.5$; $S/d = 10.5$); (**d**) *Case* 4 ($d = 3.0$ mm; $P/d = 2.8$; $S/d = 8.4$).

Additionally, the correction coefficients in the mainstream temperature correction model increased as the blowing ratio decreased, resulting in better agreement with the experimental results.

Figure 13b–d illustrate the cooling efficiency predictions for *Case* 2, *Case* 3, and *Case* 4 using the mainstream temperature correction model combined with the equivalent blowing ratio. The comparison shows that both *Case* 2 and *Case* 3 exhibited good agreement with experimental results at higher hole row counts. In *Case* 4, the prediction accuracy improved at lower blowing ratios; however, when the blowing ratio exceeded 0.64, the prediction accuracy decreased compared to the traditional Sellers model.

Compared to the Sellers prediction model, the mainstream temperature correction model did not significantly improve the prediction accuracy of the cooling efficiency at a small number of hole rows. However, as the number of hole rows increased, the improvement in the cooling efficiency prediction became increasingly significant, and the deviation from the experimental results was markedly reduced.

The reasons for this phenomenon are primarily as follows:

(a) The mainstream temperature has a relatively small effect on the cooling efficiency when the hole rows are small, due to the fact that the lateral and streamwise spreading of film cooling is limited with a small hole row. Thus, it leads to only minor differences in the cooling efficiency predictions of the two models, and both tend to overestimate compared to the experimental values.

(b) The influence of the mainstream temperature correction starts to accumulate as the number of hole rows increases. The mainstream temperature correction model takes into account the interactions between multiple film cooling rows and their complex

flow characteristics when the hole rows increase. This makes the predicted results more consistent with the experimental results.

(c) The mainstream temperature correction coefficients gradually increase as the blowing ratio decreases, which means that the mainstream temperature correction model can better capture the interactions between the film and the mainstream at lower blowing ratios, making the predictions closer to the experimental results.

#### 4.3.2. Spanwise Average Cooling Efficiency Prediction

Figure 14 presents a comparison between the predicted area-averaged cooling efficiency $\eta_{ave,L}$ and the experimental results, as defined by Equation (15). The square markers represent the spanwise-averaged cooling efficiency results for each infrared window. Although the results from different windows are not continuous, they effectively illustrate the distribution of the spanwise-averaged cooling efficiency along the streamwise direction.

$$\eta_{ave,L} = \int \eta(x,y)dy, \tag{15}$$

where $\eta(x,y)$ represents the film cooling efficiency at a specific point on the wall, obtained from infrared measurements, where $x$ denotes the streamwise direction and $y$ denotes the spanwise direction.

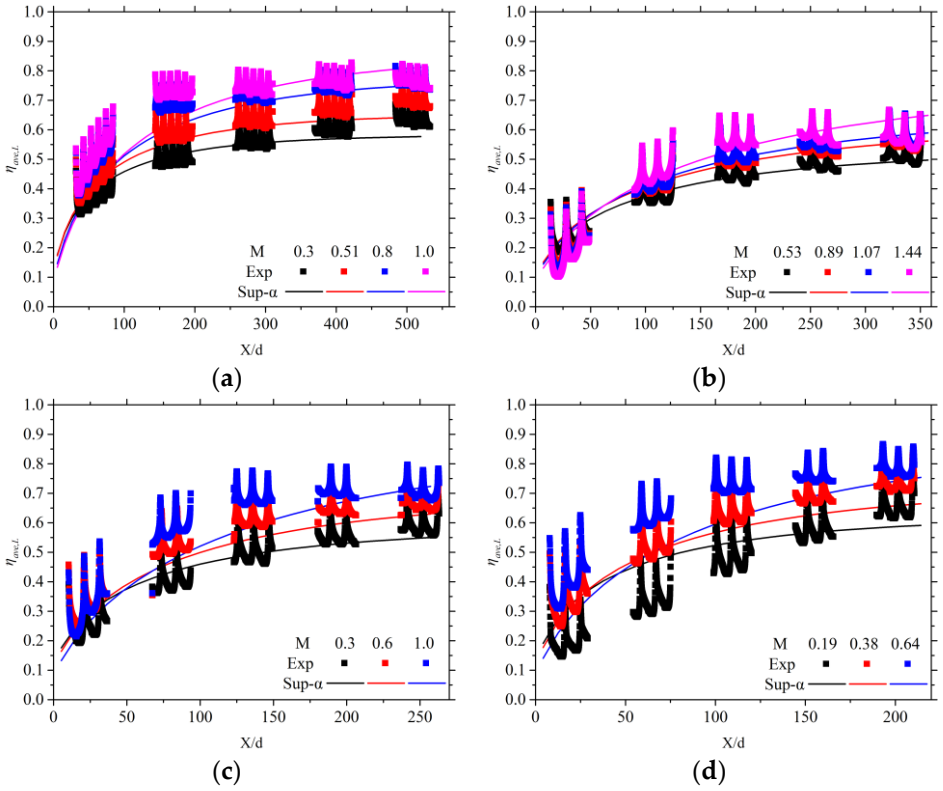



**Figure 14.** Comparison of the superposition model based on the mainstream temperature correction model ($Sup-\alpha$)-predicted spanwise-average cooling efficiency ($\eta_{ave,L}$) and the experimental results ($Exp$) along the non-dimensional streamwise distance ($X/d$) for different test plates at various blowing ratios ($M$): (**a**) *Case* 1 ($d$ = 1.2 mm; $P/d$ = 3.5; $S/d$ = 10.5); (**b**) *Case* 2 ($d$ = 1.8 mm; $P/d$ = 4.7; $S/d$ = 14); (**c**) *Case* 3 ($d$ = 2.4 mm; $P/d$ = 3.5; $S/d$ = 10.5); (**d**) *Case* 4 ($d$ = 3.0 mm; $P/d$ = 2.8; $S/d$ = 8.4).

Overall, the predicted cooling efficiency based on the mainstream temperature correction model showed good agreement with the experimental results for the spanwise-averaged cooling efficiency. For *Case* 1 and *Case* 4, the prediction performance was essen-

tially the same as the prediction performance at the centerline position. In *Case* 2, when the blowing ratio was 1.44, the cooling efficiency along the flow direction exhibited a slight decrease at high hole counts. Similarly, in *Case* 3, when the blowing ratio was one, a slight decrease in the cooling efficiency was observed, resulting in an overestimation by the prediction model.

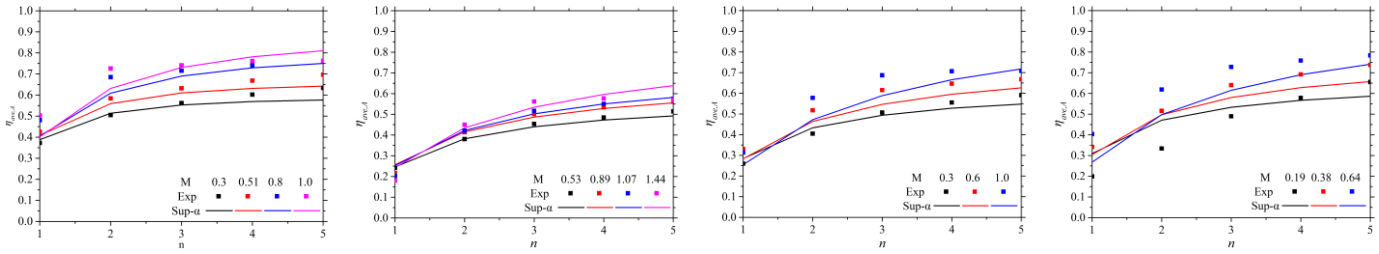
The reason for this phenomenon is that the accumulation of the cooling film leads to the formation of separation bubbles, which intensify the mixing between the mainstream flow and the cooling film at this location. This causes the cooling efficiency to decrease compared to the ideal scenario, altering the original development trend of the film. However, the prediction model has limitations in terms of accounting for flow separation and reattachment characteristics, which result in an overestimation of the cooling efficiency.

#### 4.3.3. Area-Averaged Cooling Efficiency Prediction

Figure 15 presents a comparison between the predicted area-averaged cooling efficiency $\eta_{ave,A}$ and the experimental results, as defined by Equation (16).

$$\eta_{ave,A} = \iint \eta(x,y)dxdy, \tag{16}$$

where $\eta(x,y)$ represents the film cooling efficiency at a specific point on the wall, obtained from infrared measurements, where $x$ denotes the streamwise direction and $y$ denotes the spanwise direction.




(**a**) (**b**) (**c**) (**d**)

**Figure 15.** Comparison of the superposition model based on the mainstream temperature correction model ($Sup-\alpha$)-predicted area-averaged cooling efficiency ($\eta_{ave,A}$) and the experimental results ($Exp$) for different test plates at various blowing ratios ($M$) for different windows ($n$): (**a**) *Case* 1 ($d$ = 1.2 mm; $P/d$ = 3.5; $S/d$ = 10.5); (**b**) *Case* 2 ($d$ = 1.8 mm; $P/d$ = 4.7; $S/d$ = 14); (**c**) *Case* 3 ($d$ = 2.4 mm; $P/d$ = 3.5; $S/d$ = 10.5); (**d**) *Case* 4 ($d$ = 3.0 mm; $P/d$ = 2.8; $S/d$ = 8.4).

In Figure 15a, it can be seen that at infrared window 1, the predicted cooling efficiency was significantly lower at blowing ratios of 0.8 and 1.0. However, as the number of rows of holes increased, the difference between the predicted and experimental cooling efficiencies gradually decreased. This was mainly influenced by the cooling efficiency levels at the film hole locations in the test results. Figure 10 shows that the maximum cooling efficiency at different blowing ratios was around 0.35. The cooling efficiency obtained from infrared imaging, being taken at the film hole locations with unblended coolant, resulted in an overestimation of the cooling efficiency at the same X/d location when averaged in the spanwise direction, as shown in Figure 14a, which led to an underestimation of the cooling efficiency in window 1. As the number of hole rows increased, this effect diminished, and the gap between the predicted and experimental results gradually narrowed.

In Figure 15b, it can be seen that at lower numbers of hole rows, the predicted cooling efficiency was similar to the experimental results. This was mainly due to the combined effect of film detachment at the leading edge and infrared imaging at higher blowing ratios and a larger hole spacing. The former reduced the cooling efficiency, while the latter increased it, leading to a combined effect where the cooling efficiency was lower than

predicted. Similarly, as in Figure 15a, as the number of hole rows increased, the difference between the predicted and experimental cooling efficiencies gradually decreased.

Since the streamwise and spanwise hole spacings in Figure 15c are the same as those in Figure 15a, the trend of the difference between the predicted and experimental cooling efficiencies was essentially the same and thus will not be further discussed here.

In Figure 15d, the predicted cooling efficiency is generally within the range of the experimental cooling efficiency, but it is higher at lower blowing ratios and lower at higher blowing ratios. At a blowing ratio of 0.19, the coolant was strongly affected by mainstream mixing, which prevented the film at the leading edge of the test plate from effectively covering the wall, resulting in a lower overall cooling efficiency. However, as the number of hole rows increased, the film achieved effective coverage, and the cooling efficiency gradually increased. At a blowing ratio of 0.64, although higher blowing ratios led to film detachment, the reduction in the spanwise hole spacing helped alleviate this issue. Additionally, the overestimation of the cooling efficiency at the film hole locations led to a cooling efficiency higher than the predicted value.

Figure 16 illustrates the relative prediction deviations, $\varepsilon$, with absolute values used for easier comparison. The definition of the relative prediction deviation is provided in Equation (17).

$$\varepsilon = \frac{\left|\eta_{ave,A,exp} - \eta_{ave,A,pred}\right|}{\eta_{ave,A,exp}}, \tag{17}$$

where $\eta_{ave,A,exp}$ and $\eta_{ave,A,pred}$ represent the area-averaged cooling efficiency predicted by the model and the experimentally obtained value, respectively.

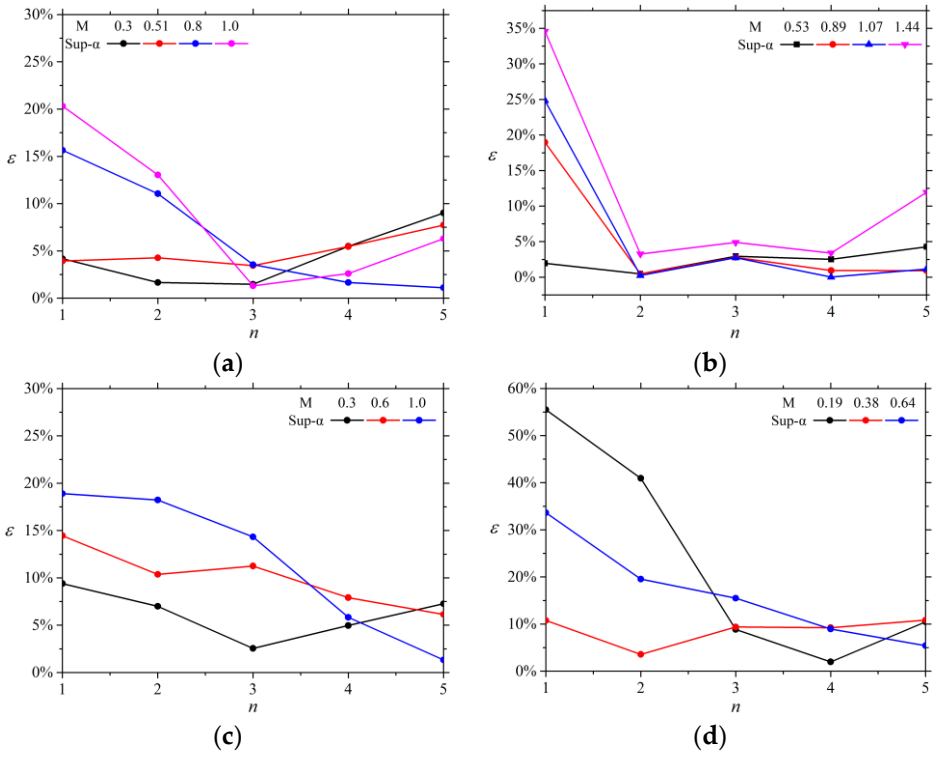



**Figure 16.** Prediction deviations ($\varepsilon$) of the area-averaged cooling efficiency ($\eta_{ave,A}$) predicted by the superposition model based on the mainstream temperature correction model ($Sup-\alpha$) for different test plates and various blowing ratios ($M$) at different windows ($n$): (**a**) *Case* 1 ($d$ = 1.2 mm; $P/d$ = 3.5; $S/d$ = 10.5); (**b**) *Case* 2 ($d$ = 1.8 mm; $P/d$ = 4.7; $S/d$ = 14); (**c**) *Case* 3 ($d$ = 2.4 mm; $P/d$ = 3.5; $S/d$ = 10.5); (**d**) *Case* 4 ($d$ = 3.0 mm; $P/d$ = 2.8; $S/d$ = 8.4).

For *Case* 1, shown in Figure 16a, the prediction deviations remained within 10% at blowing ratios of $M = 0.3$ and $M = 0.51$. However, as the blowing ratio increased to 0.8–1.0, the prediction deviation at the first window rose to 15–20%, while for the second window, it increased to between 10% and 15%. For other windows, the deviation remained within 10%.

For *Case* 2, shown in Figure 16b, the prediction deviations were generally within 10% for all windows except the first one. At this position, the deviations exceeded 15% when the blowing ratio was between 0.51 and 1.0, further increasing to over 30% at a blowing ratio of 1.0.

For *Case* 3, shown in Figure 16c, the prediction deviations remained within 10% at a blowing ratio of 0.3. However, as the ratio increased, the deviations for small hole row counts gradually rose. At a blowing ratio of 0.6, the prediction deviation for the first window increased to 10–15%, and at $M = 1.0$, it rose to 15–20%. Conversely, as the number of hole rows increased, the prediction deviations decreased. For the fourth and fifth windows, the deviations remained below 10% under various blowing ratios.

For *Case* 4, shown in Figure 16d, the prediction accuracy for small hole row counts showed significant deviations. At a blowing ratio of 0.3, the deviation reached approximately 55%. This was primarily due to the stronger influence of the mainstream flow on the film at very low blowing ratios, where the equivalent blowing ratio tended to overestimate the cooling efficiency distribution along a single row of holes. As the film layers continued to accumulate, their ability to resist mainstream interference improved, resulting in a gradual reduction in prediction deviations. Across different blowing ratios, the prediction deviations for the fourth and fifth windows remained within 10%.

Overall, for a large number of hole rows, the prediction model based on mainstream temperature correction effectively predicted the cooling efficiency of the film, with deviations remaining within 10%.

For lower hole row counts, the limitations of single-hole-row characteristics hindered accurate matching with experimental results, leading to slightly higher prediction deviations compared to those for larger hole row counts. The prediction model performed well at low blowing ratios, but as the blowing ratio increased, the prediction deviations gradually rose, reaching about 20% when the blowing ratio was one.

When the dimensional spacing of holes was modified by increasing the hole diameter, the experiments revealed significant reductions in the cooling efficiency as the blowing ratio decreased to a certain threshold. However, the prediction model failed to capture this pronounced mixing phenomenon, resulting in a rapid increase in prediction deviations.

### *4.4. Comparison with Other Predictive Models*

To further validate the effectiveness of the model, a comparison was conducted with the model proposed by Zhang et al. [38], which represents the most recent model for predicting the film cooling efficiency under high hole row counts. *Case* 1 from this study and *Case* 14 from the reference are discussed.

Figure 17 shows the predictions of the film cooling efficiency along the flow direction for *Case* 1 using various models. Overall, the literature models tended to overestimate the cooling efficiency at the centerline position along the flow direction. The variation in the predicted cooling efficiency across different blowing ratios was relatively small. Compared to the model proposed in this study, the predictions of the cooling efficiency at the experiment's centerline position were less accurate.

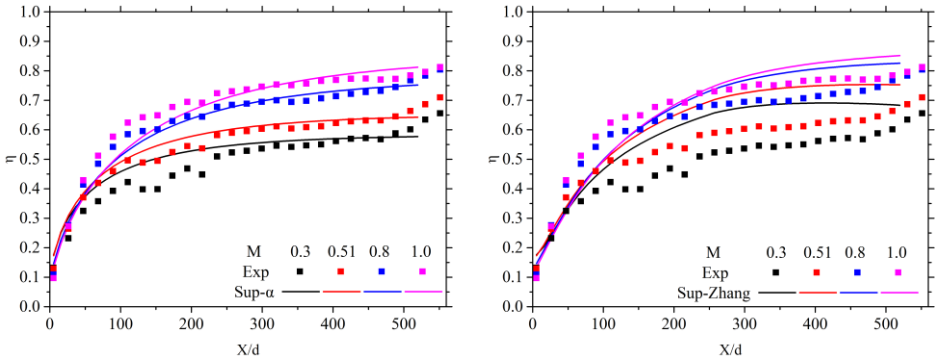



**Figure 17.** Comparison of the superposition model based on the mainstream temperature correction model ($Sup-\alpha$)-predicted centerline cooling efficiency ($\eta$) and Zhang's model ($Sup-Zhang$)-predicted results along the non-dimensional streamwise distance ($X/d$) for *Case* 1 of this study ($d = 1.2$ mm; $P/d = 3.5$; $S/d = 10.5$). (**a**) Predicted results using the superposition model based on mainstream temperature correction ($Sup-\alpha$). (**b**) Predicted results using Zhang's model ($Sup-Zhang$).

Figure 18 compares the spanwise-averaged cooling efficiency predictions for *Case* 14 in the reference using different models. At a blowing ratio of 0.3, the model proposed in this study overpredicted the cooling efficiency at lower hole row counts; however, the prediction accuracy improved as the number of hole rows increased. As the blowing ratio increased, the reference model significantly overestimated the film coverage on the wall, resulting in a higher predicted cooling efficiency, whereas the model proposed in this study showed better agreement with the experimental results.

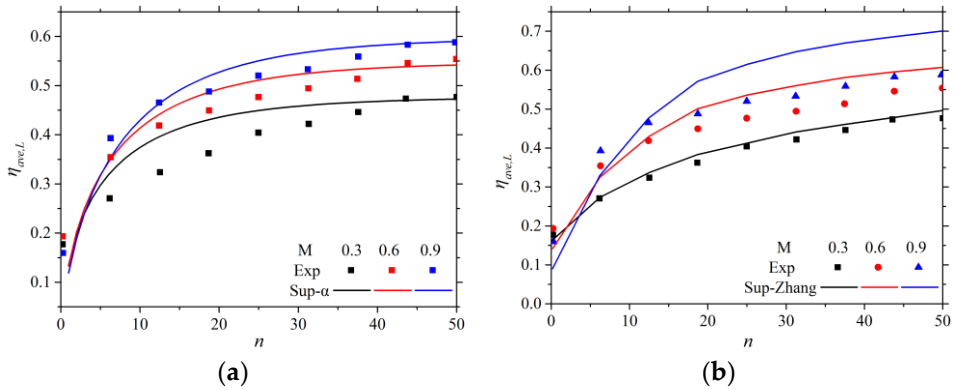



**Figure 18.** Comparison of the superposition model based on mainstream temperature correction ($Sup-\alpha$)-predicted spanwise-averaged cooling efficiency ($\eta_{ave,L}$) and Zhang's model ($Sup-Zhang$)-predicted results along the non-dimensional streamwise direction ($X/d$) for *Case* 14 of Zhang's study ($d = 1$ mm; $P/d = 4$; $S/d = 16$): (**a**) predicted results using the superposition model based on mainstream temperature correction ($Sup-\alpha$); (**b**) predicted results using Zhang's model ($Sup-Zhang$).

Table 5 compares the prediction deviations of two film cooling superposition models under different blowing ratios.

For *Case* 1 in this study, the model proposed in this study and the existing literature model exhibited similar deviation trends across different blowing ratios, but significant differences exist in the specific deviation values. As the blowing ratio increased, the prediction deviation of this study's model remained between −2.1% and 7.3%, while the literature model showed deviations ranging from 0.5% to 22.8%. This difference in deviation ranges indicates that the model from this study has higher accuracy and

stability across a broader range of conditions. In contrast, the literature model may exhibit considerable uncertainty under certain conditions, significantly impacting its reliability in practical applications.

**Table 5.** Comparison of area-averaged cooling efficiency forecast deviations.

| Predictive Model | *Case* 1 in This Study | | | | *Case* 14 in Zhang's Study | | |
|---|---|---|---|---|---|---|---|
| | $M = 0.3$ | $M = 0.5$ | $M = 0.8$ | $M = 1.0$ | $M = 0.3$ | $M = 0.6$ | $M = 0.9$ |
| This study | 7.3% | 3.4% | −0.8% | −2.1% | 9.7% | 3.4% | 2.2% |
| Zhang et al. [38] | 22.8% | 16.1% | 5.4% | 0.5% | 3.0% | 8.0% | 12.7% |

For *Case* 14 in Zhang's study, the prediction deviation of the model proposed in this study similarly decreased with increasing blowing ratios, whereas the literature model showed the opposite trend. At $M = 0.3$, the literature model exhibited a lower deviation; however, as the blowing ratio increased, the deviation rose significantly, reaching 12.7% at $M = 0.9$, which is notably higher than that of this study's model. This further demonstrates the accuracy of the model proposed in this study under most conditions, particularly under high blowing ratios, where its performance is notably superior.

## 5. Conclusions

In designing a turbine outer ring with film cooling, accurately predicting the cooling efficiency of multiple rows of film holes along the flow direction can significantly reduce the design iteration time. Therefore, developing a reliable superposition prediction method is crucial. However, most existing methods are limited to cases with a small number of rows, assume constant flow temperatures, and rely on pre-determined single-row characteristics. Research on superposition models for cases involving many rows, varying flow temperatures, or limited single-row data remains insufficient. Further studies are needed to develop an effective superposition prediction method for turbine outer ring surfaces.

This study developed a superposition prediction model based on mainstream temperature correction from an energy conservation perspective, using a single fixed hole spacing. Under the assumption of an equivalent blowing ratio, the model enables film cooling efficiency prediction with minimal cooling efficiency data requirements. A dimensionless temperature parameter was introduced to account for mainstream and secondary flow variations at different positions.

Additionally, four different structural configurations of film cooling efficiency experiments were conducted to validate the prediction model, which was also compared with an existing film superposition correction model. The results indicate that the corrected prediction model shows good agreement with experimental results. The following conclusions were drawn from this study.

1. The existing Sellers method accumulates prediction errors as the number of hole rows increases, resulting in an overestimation of the cooling efficiency compared to experimental results. Although using an equivalent blowing ratio in the Sellers method helps the predicted distribution range align more closely with experimental data, it still tends to underestimate the variation in the cooling efficiency across different blowing ratios while overestimating the film cooling efficiency at different positions.
2. Introducing a mainstream temperature correction factor effectively addresses the overestimation of the cooling efficiency in the prediction model. This correction improves the accuracy of predictions across various blowing ratios, resulting in better agreement with experimental data. In most cases, the prediction accuracy is higher at lower blowing ratios and with a larger number of hole rows.

3. Compared to existing models in the literature, the proposed model demonstrates higher prediction accuracy under most conditions. It provides a simplified modified model that can be easily applied in the design of turbine outer rings and other similar structures with film cooling.

Compared to existing film cooling superposition models, the proposed model incorporates more design factors, including variations in the mainstream and coolant temperatures along the flow direction, the equivalent blowing ratio method when film cooling distribution characteristics are unavailable, and a model correction approach based on energy conservation that breaks the assumption of film independence. This model offers the potential for rapid design in the early stages of complex structure development and demonstrates strong applicability in mixed-dimensional coupled designs of complex components (e.g., integrating low-dimensional film cooling models with high-dimensional heat transfer models). While the empirical coefficients in this model cannot fully cover all film cooling structures and operating conditions, the model provides valuable design references for other structural configurations.

**Author Contributions:** All the authors have contributed to this research. Conceptualization and methodology, Z.G., T.Q., P.L. and S.D.; software, Z.G. and Z.L.; validation, formal analysis, investigation, and data curation, Z.G., Z.L., Q.Y. and R.C.; writing—original draft, Z.G., T.Q., P.L., S.D., Z.L., Q.Y. and R.C. All authors have read and agreed to the published version of the manuscript.

**Funding:** The National Science and Technology Major Project of China (Grant No. J2019-III-0003-0046).

**Data Availability Statement:** The raw data supporting the conclusions of this article will be made available by the authors on request.

**Conflicts of Interest:** This research did not receive any specific grant from funding agencies in the public, commercial, or not-for-profit sectors. The authors declare no conflicts of interest.

## Nomenclature

| | | | |
|---|---|---|---|
| $A$ | area | $a$ | empirical coefficient $a$ |
| $b$ | empirical coefficient $b$ | $C$ | empirical coefficient $C$ |
| $d$ | diameter | $Exp$ | experiment |
| $H$ | height of the test plate | $L$ | length of the test plate |
| $IR$ | infrared | $TC$ | thermocouple temperature |
| $M$ | blowing ratio | $m$ | mass flow rate |
| $n$ | infrared window index | $P$ | pitch of holes |
| $Sup-s$ | Sellers superposition model | $S$ | hole spacing |
| $Sup-s-M$ | Sellers superposition model with equivalent bleed ratio | | |
| $Sup-\alpha$ | superposition model based on mainstream temperature correction | | |
| $s$ | slot width | $T$ | temperature |
| $u$ | velocity | $W$ | width of the test plate |
| $X$ | distance from the origin along the streamwise direction | | |
| $\alpha$ | mainstream temperature correction factor | | |
| $\varepsilon$ | error value | $\eta$ | film cooling efficiency |
| $\xi$ | dimensionless temperature | $\rho$ | density |

| | | | |
|---|---|---|---|
| **Subscripts** | | | |
| 0 | initial state | 1 | film hole row 1 |
| 2 | film hole row 2 | *ave*, *A* | area average |
| *ave*, *L* | line average | *aw* | adiabatic wall |
| *c* | coolant | *e* | equivalent state |
| *exp* | experiment result | *g* | mainstream |
| *i* | film hole row *i* | *j* | film hole row *j* |
| *k* | film hole row *k* | *max* | maximum value |
| *min* | minimum value | *n* | film hole row *n* |
| *pred* | prediction result | | |
| **Superscripts** | | | |
| ′ | modified parameters | | |

## References


1. Zhang, J.; Zhang, S.; Wang, C.; Tan, X. Recent advances in film cooling enhancement: A review. *Chin. J. Aeronaut.* **2020**, *33*, 1119–1136. [CrossRef]
2. Wang, W.; Yan, Y.; Zhou, Y.; Cui, J. Review of Advanced Effusive Cooling for Gas Turbine Blades. *Energies* **2022**, *15*, 8568. [CrossRef]
3. Baek, S.I.; Ahn, J. Large Eddy Simulation of Film Cooling with Triple Holes: Injectant Behavior and Adiabatic Film-Cooling Effectiveness. *Processes* **2020**, *8*, 1443. [CrossRef]
4. Baek, S.I.; Ahn, J. Large Eddy Simulation of Film Cooling Involving Compound Angle Holes: Comparative Study of LES and RANS. *Processes* **2021**, *9*, 198. [CrossRef]
5. Ravelli, S.; Barigozzi, G. Numerical evaluation of heat/mass transfer analogy for leading edge showerhead film cooling on a first-stage vane. *Int. J. Heat Mass Transf.* **2019**, *129*, 842–854. [CrossRef]
6. Wang, H.; Tao, Z.; Zhou, Z.; Han, F.; Li, H. Experimental and numerical study of the film cooling performance of the suction side of a turbine blade under the rotating condition. *Int. J. Heat Mass Transf.* **2019**, *136*, 436–448. [CrossRef]
7. Collopy, H.; Ligrani, P.M.; Xu, H.; Fox, M. Effects of pressure side film cooling hole placement and condition on adiabatic film cooling effectiveness characteristics of a transonic turbine blade tip. *Int. J. Heat Mass Transf.* **2022**, *199*, 123462. [CrossRef]
8. Wang, N.; Shiau, C.-C.; Han, J.-C.; Xu, H.; Fox, M. Turbine vane endwall film cooling from mid-chord or downstream rows and upstream coolant injection. *Int. J. Heat Mass Transf.* **2019**, *133*, 247–255. [CrossRef]
9. Li, Z.; Xie, P.; Zeng, Q.; Chen, X. Study of Tangential Effusion Cooling of a Combustor Liner. *Processes* **2023**, *11*, 2433. [CrossRef]
10. Li, Z.; Wang, L.; Mao, J.; Bi, S.; Wang, F. Experimental Study on Impingement and Film Overall Cooling Characteristics of Turbine Shroud. *J. Therm. Sci.* **2022**, *31*, 239–250. [CrossRef]
11. Lee, C.-P.; Robinson, G.D.; Orlando, R.J. Duplex Turbine Shroud. U.S. Patent 8104292B2, 31 January 2012.
12. Cui, H.; Wang, L.; Li, X.; Ren, J. Data-Driven Conjugate Heat Transfer Analysis of a Gas Turbine Vane. *Processes* **2022**, *10*, 2335. [CrossRef]
13. Sellers, J.P., Jr. Gaseous film cooling with multiple injection stations. *AIAA J.* **1963**, *1*, 2154–2156. [CrossRef]
14. Muska, J.F.; Fish, R.W.; Suo, M. The Additive Nature of Film Cooling from Rows of Holes. *J. Eng. Power* **1976**, *98*, 457–463. [CrossRef]
15. Mhetras, S.; Han, J.-C. Effect of Superposition on Spanwise Film-Cooling Effectiveness Distribution on a Gas Turbine Blade. In Proceedings of the ASME 2006 International Mechanical Engineering Congress and Exposition, Chicago, IL, USA, 5–10 November 2006; pp. 477–487.
16. Mhetras, S.; Han, J.-C.; Rudolph, R. Film-Cooling Effectiveness from Shaped Film Cooling Holes for a Gas Turbine Blade. In Proceedings of the ASME Turbo Expo 2008: Power for Land, Sea, and Air, Berlin, Germany, 9–13 June 2008; pp. 837–848.
17. Wang, P.F.; Xu, Q.Z.; Liu, J.; Wang, P.; Du, Q.; Wang, Z.G. Experimental and unsteady numerical investigations on cooling characteristics of trailing-edge cutback with effect of upstream film holes. *Int. J. Therm. Sci.* **2023**, *193*, 108423. [CrossRef]
18. Sasaki, M.; Takahara, K.; Kumagai, T.; Hamano, M. Film Cooling Effectiveness for Injection from Multirow Holes. *J. Eng. Power* **1979**, *101*, 101–108. [CrossRef]
19. Meng, T.; Zhu, H.-r.; Liu, C.-l.; Wei, J.-s. Investigation on the Accuracy of Superposition Predictions of Film Cooling Effectiveness. *Int. J. Turbo Jet-Engines* **2018**, *35*, 181–192. [CrossRef]
20. Li, B.; Liu, C.; Ye, L.; Zhou, T. Evaluation of Film Cooling Effect in Multi-Row Hole Configurations on Turbine Blade Leading Edge. *Energy* **2024**, *309*, 132908. [CrossRef]

21. Li, B.-r.; Zhou, T.-l.; Liu, C.-l.; Ye, L.; Zhang, F. Showerhead Film Cooling Mechanism and Superposition Characteristics of Turbine Blade Leading-Edge. In Proceedings of the ASME Turbo Expo 2024: Turbomachinery Technical Conference and Exposition, London, UK, 24–28 June 2024.
22. Anderson, J.B.; Winka, J.R.; Bogard, D.G.; Crawford, M.E. Evaluation of Superposition Predictions for Showerhead Film Cooling on a Vane. *J. Turbomach.* **2014**, *137*, 041010. [CrossRef]
23. Takeishi, K.; Oda, Y.; Nagao, T.; Sakamoto, H. Superposition method for multi rows of a film cooling hole on a turbine stationary vane surface. *Heat Transf. Xiv Simul. Exp. Heat Transf. Its Appl.* **2016**, *106*, 11–24.
24. Wang, L.; Li, X.; Ren, J.; Jiang, H. Effect of Row Spacing on the Accuracy of Film Cooling Superposition Method. In Proceedings of the ASME Turbo Expo 2018: Turbomachinery Technical Conference and Exposition, Oslo, Norway, 11–15 June 2018; pp. 463–472.
25. Murray, A.V.; Ireland, P.T.; Wong, T.H.; Tang, S.W.; Rawlinson, A.J. High resolution experimental and computational methods for modelling multiple row effusion cooling performance. *Int. J. Turbomach. Propuls. Power* **2018**, *3*, 4. [CrossRef]
26. Huo, T.Y.; Xing, J.J.; Han, S.H.; Guo, T.R.; Li, L.; Du, X.Z.; Zhang, R.S.; Zhou, L.P.; Zhang, H. Accurate predictions of mist assisted film cooling characteristics and effectiveness on a flat plate with double-row holes. *Int. J. Heat Mass Transf.* **2024**, *227*, 125595. [CrossRef]
27. Chen, Z.; Li, Y.; Su, X.; Yuan, X. Accuracy Assessment of the Sellers Model in Predicting the Multi-Row Film cooling Performance. In Proceedings of the ASME Turbo Expo 2020: Turbomachinery Technical Conference and Exposition, Virtual Online, 21–25 September 2020.
28. Liu, H.; Du, Q.; Xu, Q.; Xu, J.; Xu, G.; Li, H.; Wang, P. Film Superposition Characteristics With Laidback Fan-Shaped Holes Under the Influence of Internal Crossflow. In Proceedings of the ASME Turbo Expo 2024: Turbomachinery Technical Conference and Exposition, London, UK, 24–28 June 2024.
29. Ethridge, M.I.; Cutbirth, J.M.; Bogard, D.G. Effects of Showerhead Cooling on Turbine Vane Suction Side Film Cooling Effectiveness. In Proceedings of the ASME 2000 International Mechanical Engineering Congress and Exposition, Orlando, FL, USA, 5–10 November 2000; pp. 69–78.
30. Polanka, M.D.; Ethridge, M.I.; Cutbirth, J.M.; Bogard, D.G. Effects of Showerhead Injection on Film Cooling Effectiveness for a Downstream Row of Holes. In Proceedings of the ASME Turbo Expo 2000: Power for Land, Sea, and Air, Munich, Germany, 8–11 May 2000.
31. Li, X.; Ren, J.; Jiang, H. Multi-row film cooling characteristics on a vane endwall. *Int. J. Heat Mass Transf.* **2016**, *92*, 23–33. [CrossRef]
32. Andreini, A.; Carcasci, C.; Gori, S.; Surace, M. Film cooling system numerical design: Adiabatic and conjugate analysis. In Proceedings of the ASME 2005 Summer Heat Transfer Conference, San Francisco, CA, USA, 17–22 July 2005; pp. 9–20.
33. Wang, L.; Li, X.; Lie, W.; Ren, J.; Jiang, H. Superposition Characteristics of Full Coverage Film Cooling with Various Blowing Ratio and Row Number. In Proceedings of the Asme Turbo Expo 2019: Turbomachinery Technical Conference and Exposition, Phoenix, AZ, USA, 17–21 June 2019.
34. Chen, Z.; Mao, Y.; Hu, K.; Su, X.; Yuan, X. 2-D prediction method for multi-row film cooling effectiveness. *Appl. Therm. Eng.* **2021**, *199*, 117607. [CrossRef]
35. Zhang, Z.; Zhu, H.R.; Liu, C.L.; Zhang, B.L.; Yao, C.Y.; Wu, Z. Effects of Holes Arrangement on the Superposition Characteristics of Film Cooling Effectiveness. *J. Thermophys. Heat Transf.* **2022**, *36*, 556–567. [CrossRef]
36. Xu, Z.; Zhu, H.; Liu, C.; Ye, L.; Zhou, D. Film Cooling Effectiveness Superposition Calculation of Double-Row Injection Holes on Turbine Vane. *J. Therm. Sci.* **2022**, *31*, 2424–2437. [CrossRef]
37. Zhang, F.; Liu, C.; Wang, W.; Ye, L.; Li, B.; Liu, F. Film superposition prediction method for film cooling layouts with same opening ratio on the turbine blade. *Appl. Therm. Eng.* **2023**, *233*, 121105. [CrossRef]
38. Zhang, F.; Liu, C.; Ye, L.; Ran, Y.; Zhou, T.; Yan, H. Study on the film superposition method for dense multirow film Hole layouts. *Energy* **2024**, *293*, 130607. [CrossRef]
39. Kirollos, B.; Povey, T. An Energy-Based Method for Predicting the Additive Effect of Multiple Film Cooling Rows. *J. Eng. Gas Turbines Power* **2015**, *137*, 122607. [CrossRef]
40. An, B.; Liu, J. Study on Additive Effect of Film Cooling Effectiveness in Two Rows of Fan-Shaped Holes. *J. Turbomach.* **2024**, *146*, 021012.
41. Berkache, A.; Amroune, S.; Jawaid, M.; Singh, B. Investigating crossflow interactions in multi-perforation cooling systems: Experimental and numerical insights. *Appl. Therm. Eng.* **2024**, *252*, 123681. [CrossRef]
42. Bogard, D.G.; Thole, K.A. Gas Turbine Film Cooling. *J. Propuls. Power* **2006**, *22*, 249–270. [CrossRef]
43. Harrington, M.K.; McWaters, M.A.; Bogard, D.G.; Lemmon, C.A.; Thole, K.A. Full-Coverage Film Cooling with Short Normal Injection Holes. In Proceedings of the ASME Turbo Expo 2001: Power for Land, Sea, and Air, New Orleans, LA, USA, 4–7 June 2001.

44. Moffat, R.J. Describing the uncertainties in experimental results. *Exp. Therm. Fluid Sci.* **1988**, *1*, 3–17. [CrossRef]
45. Eckert, E.; Goldstein, R.; Ramsey, J. Film Cooling with Injection Through a Circular Hole Summary Report. NASA-CR-54604; NASA Lewis Research Center: Cleveland, OH, USA, 1968.

**Disclaimer/Publisher's Note:** The statements, opinions and data contained in all publications are solely those of the individual author(s) and contributor(s) and not of MDPI and/or the editor(s). MDPI and/or the editor(s) disclaim responsibility for any injury to people or property resulting from any ideas, methods, instructions or products referred to in the content.